NAVAL POSTGRADUATE SCHOOL

MONTEREY, CALIFORNIA

THESIS

DIRECT NUMERICAL SIMULATIONS OF THE DIFFUSIVE CONVECTION AND ASSESSMENT OF ITS IMPACT ON ARTIC CLIMATE CHANGE

by

Ivo J. Prikasky

September 2007

Thesis Advisor:	Timour Radko
Second Reader:	William Shaw

Approved for public release; distribution is unlimited

THIS PAGE INTENTIONALLY LEFT BLANK

REPORT DOCUMENTATION PAGE		Form Approved OMB No. 0704-0188

1. AGENCY USE ONLY *(Leave blank)*	2. REPORT DATE	3. REPORT TYPE AND DATES COVERED
	September 2007	Master's Thesis

4. TITLE AND SUBTITLE
Direct Numerical Simulations of the Diffusive Convection and Assessment of Its Impact on Artic Climate Change.

6. AUTHOR(S) Ivo J. Prikasky

7. PERFORMING ORGANIZATION NAME(S) AND ADDRESS(ES)	8. PERFORMING ORGANIZATION REPORT NUMBER
Naval Postgraduate School Monterey, CA 93943-5000	

9. SPONSORING /MONITORING AGENCY NAME(S) AND ADDRESS(ES)	10. SPONSORING/MONITORING AGENCY REPORT NUMBER
N/A	

11. SUPPLEMENTARY NOTES The views expressed in this thesis are those of the author and do not reflect the official policy or position of the Department of Defense or the U.S. Government.

12a. DISTRIBUTION / AVAILABILITY STATEMENT	12b. DISTRIBUTION CODE
Approved for public release; distribution is unlimited	

13. ABSTRACT (maximum 200 words)

This thesis focuses on the numerical modeling of the oceanic double-diffusive convection, a mixing process which is driven by the two orders of magnitude difference in diffusivities of heat and salt in seawater. This study explores the diffusive regime of double-diffusion. The aim of the research is to quantify the double-diffusive transport in both smooth gradients and thermohaline staircases, and to develop clear insight into the origin of the staircases and specify conditions for their formation. Based on the numerical process modeling, it is determined that the evolutionary pattern of staircases is controlled by the merging events in which weak interfaces erode and disappear. To illustrate dynamics of these events, a theoretical framework – merging theorem – has been developed. It is numerically confirmed that the merging theorem predicts the time scale of merging events within the order of magnitude. The computed fluxes from numerical experiments are comparable to the diffusive fluxes inferred from the Beaufort Gyre observations and an order of magnitude greater than the fluxes from earlier laboratory-based experiments. The present analysis suggests that the diffusive fluxes could play an important factor in the Arctic heat budget; hence, future study in this field is recommended.

14. SUBJECT TERMS	15. NUMBER OF PAGES
double-diffusion, diffusive convection, flux, thermohaline staircase, merging	81
	16. PRICE CODE

17. SECURITY CLASSIFICATION OF REPORT	18. SECURITY CLASSIFICATION OF THIS PAGE	19. SECURITY CLASSIFICATION OF ABSTRACT	20. LIMITATION OF ABSTRACT
Unclassified	Unclassified	Unclassified	UU

NSN 7540-01-280-5500 Standard Form 298 (Rev. 2-89)
Prescribed by ANSI Std. 239-18

THIS PAGE INTENTIONALLY LEFT BLANK

Approved for public release; distribution is unlimited

DIRECT NUMERICAL SIMULATIONS OF THE DIFFUSIVE CONVECTION AND ASSESSMENT OF ITS IMPACT ON ARTIC CLIMATE CHANGE

Ivo J. Prikasky
Lieutenant Commander, United States Navy
B.A., Binghamton University, 1995

Submitted in partial fulfillment of the
requirements for the degree of

MASTER OF SCIENCE IN METEOROLOGY & PHYSICAL OCEANOGRAPHY

from the

NAVAL POSTGRADUATE SCHOOL
SEPTEMBER 2007

Author: Ivo J. Prikasky

Approved by: Timour Radko
Thesis Advisor

William Shaw
Second Reader

Mary L. Batteen,
Chairperson, Department of Oceanography

THIS PAGE INTENTIONALLY LEFT BLANK

ABSTRACT

This thesis focuses on the numerical modeling of the oceanic double-diffusive convection, an important small-scale mixing process which is driven by the two orders of magnitude difference in diffusivities of heat and salt in seawater. This study explores the diffusive regime of double-diffusion which is realized when cold and fresh water overlies the warm and salty water.

The aim of the research was to quantify the double-diffusive transport in both smooth gradients and thermohaline staircases, and to develop clear insight into the origin of the staircases and specify conditions for their formation. Based on the numerical process modeling, it was determined that the evolutionary pattern of staircases is controlled by the merging events in which weak interfaces gradually erode and ultimately disappear. To illustrate dynamics of these events, a theoretical framework – merging theorem – has been developed. It was numerically confirmed that the merging theorem predicts the time scale of merging events within the order of magnitude. The validity of the lab derived 4/3 flux law was tested and it was determined that its form is consistent with the numerical results, but the amplitude requires adjustment.

The computed fluxes from numerical experiments were comparable to the diffusive fluxes that were inferred from the Beaufort Gyre observations(Wilson, 2007) and an order of magnitude greater than the fluxes from earlier laboratory-based experiments.

Although a large discrepancy in the values of diffusive fluxes exists in the earlier laboratory and field studies,

the present analysis suggests that the diffusive fluxes could play an important factor in the Arctic heat budget; hence, future study in this field is recommended.

This study contributes to a better understanding of global climate change, which presents a new challenge to national security. The Navy has to be concerned with the impact of climate change on naval operations, specifically in the Arctic where the melting polar ice cap may soon provide a gateway across the north, resulting in the opening of shipping lanes and borders.

TABLE OF CONTENTS

THIS PAGE INTENTIONALLY LEFT BLANK

LIST OF FIGURES

LIST OF TABLES

THIS PAGE INTENTIONALLY LEFT BLANK

ACKNOWLEDGMENTS

I take this opportunity to express my gratitude and indebtedness to those without whose assistance this project would never came about. I thank my wife and children for their continual love, support, and patience, they are inspiration for everything I do. I thank my Thesis Advisor, Dr. Timour Radko for assistance, patience, and expertise rendered in all aspects of this project. I thank Dr. William Shaw, my second reader, for helpful comments. I thank Dr. Jeffrey Haferman for his help with all aspects of information technology. I thank Mike Cook for assistance with Matlab.

I also gratefully acknowledge my officemates Ana Wilson, Alban Simon, and Steven Wall, who offered encouragement, helpful comments and countless help during all stages of this project.

THIS PAGE INTENTIONALLY LEFT BLANK

I. INTRODUCTION

A. DESCRIPTION OF DOUBLE-DIFFUSIVE PROCESS

1. Importance of Double-diffusive Process

The significance of double-diffusive mixing and its effect on various large oceanic features has become a major driving force for much of oceanographic research in this field over the last few decades. In this thesis two important aspects are explored: (1) the mechanics of diffusive staircases and (2) the possibility that vertical heat fluxes, which are driven by the diffusive convection, play a significant role in the maintenance of the Arctic thermocline and melting rates of the polar ice cap.

2. Double-diffusive Process - Introduction

Double-diffusive convection may occur in a stratified fluid if its density is determined by two or more constituents with different molecular diffusivities. This process is commonly observed in the ocean where the diffusivity of heat is about 100 times greater than the diffusivity of salt (typical value of the molecular diffusivity of heat ~ 1.4×10^{-7} $m^2 s^{-1}$, and that of salt ~ 1.1×10^{-9} $m^2 s^{-1}$). Since heat diffuses much faster than salt, the resulting instability is vigorous and often leads to elevated mixing. Double-diffusive convection was first discovered by Henry Stommel (Stommel et al.,1956) and Melvin Stern (Stern, 1960).

3. Salt-finger Regime of Double-diffusive Process

Two modes of the double-diffusive process are known: the salt-finger regime and the diffusive convection. To understand the salt-finger mode, consider a case in the ocean where a warm and salty layer of water overlies a colder and fresher layer of water, the bottom layer having a higher density than the top layer. In the absence of molecular diffusion, if a parcel of water is displaced downward by some force from the lower density layer into the higher density layer, it tends to return to its initial position due to buoyancy force. However the situation becomes very different when diffusion is taken into account. Instead, due to the higher diffusivity of heat, the parcel will become denser (and heavier) than the surrounding water and will continue to sink further. As a result, narrow, elongated vertical structures are formed, which are commonly referred to as salt fingers.

The faster diffusing component (heat) is stabilizing, and the slower diffusing component (salt) is destabilizing. The regions favorable for the salt finger regime include the tropics and subtropics where both the temperature and salinity decrease with depth. According to Schmitt (1990), 90% of the upper kilometer of the Atlantic at 24 degrees North is favorable to salt finger formation.

Other favorable regions are semi-enclosed seas which outflow into the ocean, such as the Mediterranean Sea and its outflow through the Straits of Gibraltar. Due to the exceedance of evaporation over precipitation in the Mediterranean, the warm and salty waters of the Mediterranean flow over the colder and fresher waters of the

Atlantic and spread out to a depth of about 1 kilometer. A numerical example is presented in Figure 1.

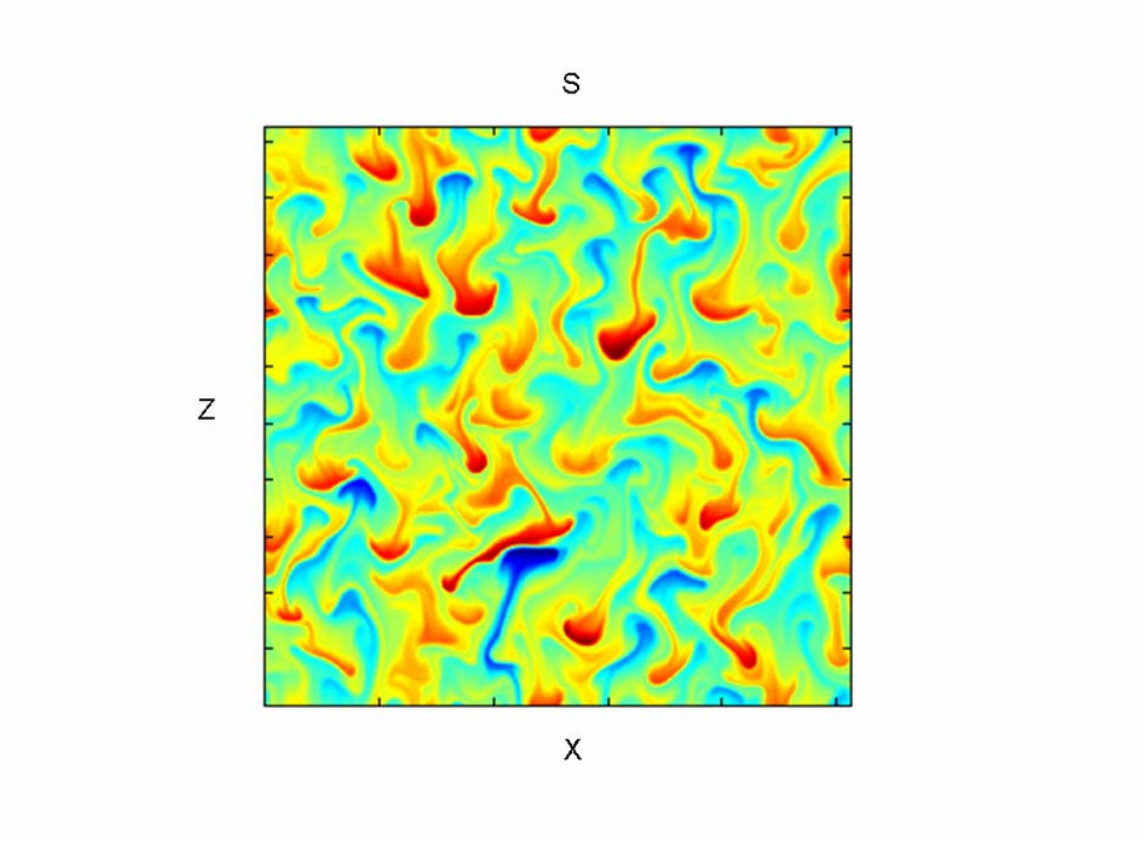

Figure 1. Numerical simulation of salt fingers. Red color corresponds to high values of salinity; low values are shown in blue.

4. Diffusive Convection Regime of Double-diffusive Process

The second regime, the diffusive convection, occurs when a cold, fresh layer overlies a warmer, saltier layer. Again, in order to preserve stability, the bottom layer has greater density than the top layer. Due to differing diffusivities of the two components, diffusive plumes grow across the interface in the vertical direction, and transport both the heat and salt between the two layers. In

this case, the faster diffusing constituent (heat) is destabilizing and provides the release of potential energy to drive the motion, and the slower diffusing constituent (salt) is stabilizing. The regions favorable for the diffusive convection include the polar and subpolar regions of the Arctic and the Southern Ocean. Here, the melting of ice and small rates of evaporation result in the colder and fresher upper layer, thereby resulting in conditions favorable to diffusive convection. A numerical example is shown in Figure 2.

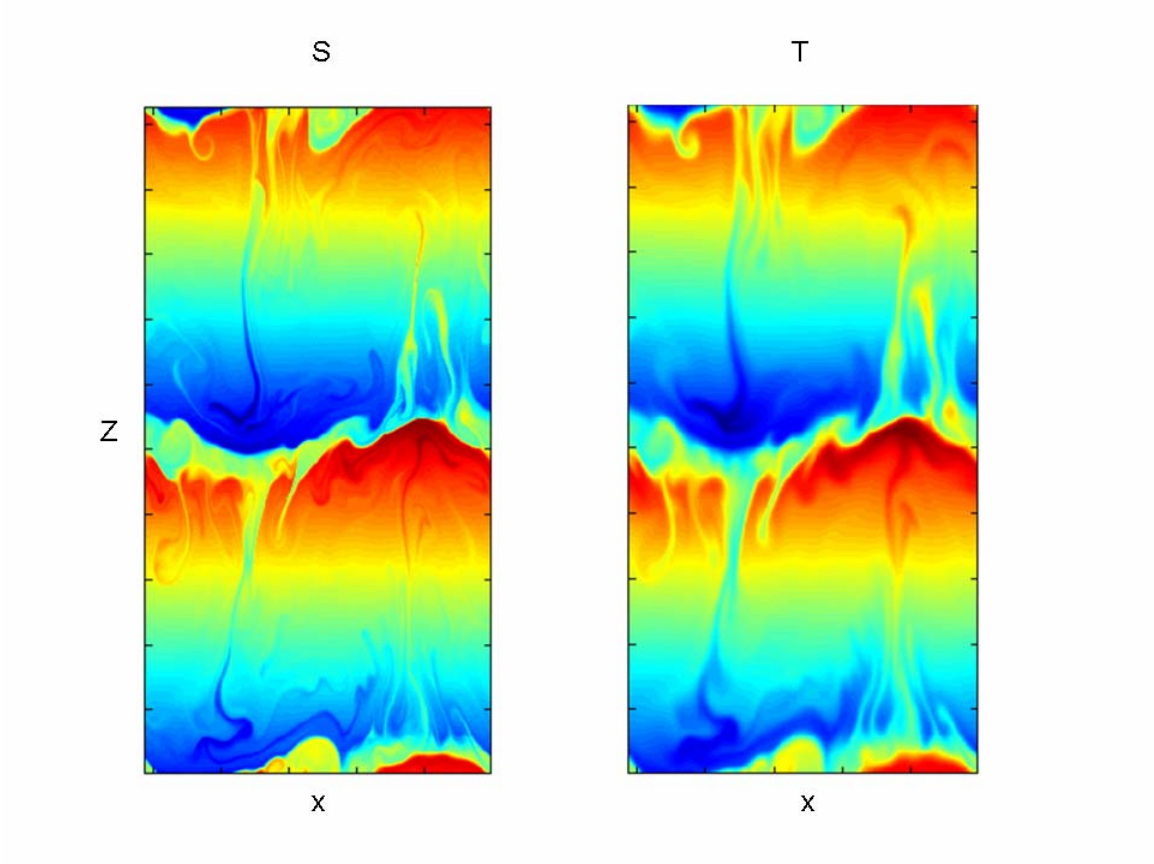

Figure 2. Diffusive convection example. Two layer system with the depiction of heat (left) and salinity (right). The high values of T and S are shown in red; low values are represented in blue.

The diffusive convection, in turn, takes two distinct forms depending on the background stratification: oscillatory convection in smooth gradients and diffusive layering. The schematic diagram in Figure 3 describes oscillatory diffusive convection. In this model, a water parcel is slightly displaced upward in a diffusively favorable environment (a cold, fresh layer overlays a warmer and saltier one). As the particle travels upwards, it will rapidly loose heat but maintain salinity. However, due to the decrease of the background salinity with depth, the

parcel becomes heavier than its surroundings, and the buoyancy force will drive it back towards the initial position. The parcel becomes heavier from the initial state not only because of the change in the density contrast with its surroundings, but also because of its heat loss. As a result, the restoring buoyancy force which drives the parcel to its initial position is now greater than the initial upward buoyancy force. The final result is a gain of energy by the parcel and subsequent oscillatory motion during which the parcel overshoots its original position of neutral equilibrium. An analogous process takes place as the parcel travels downward below its initial position. It now gains heat, but maintains salinity, and since the parcel is fresher and lighter, it will experience an upward buoyancy force and overshoot its initial position. The whole cycle will be repeated time and again, with an increase of energy within the parcel and the growth of oscillations over time. This instability pattern is sometimes referred to as the “over-stable” mode.

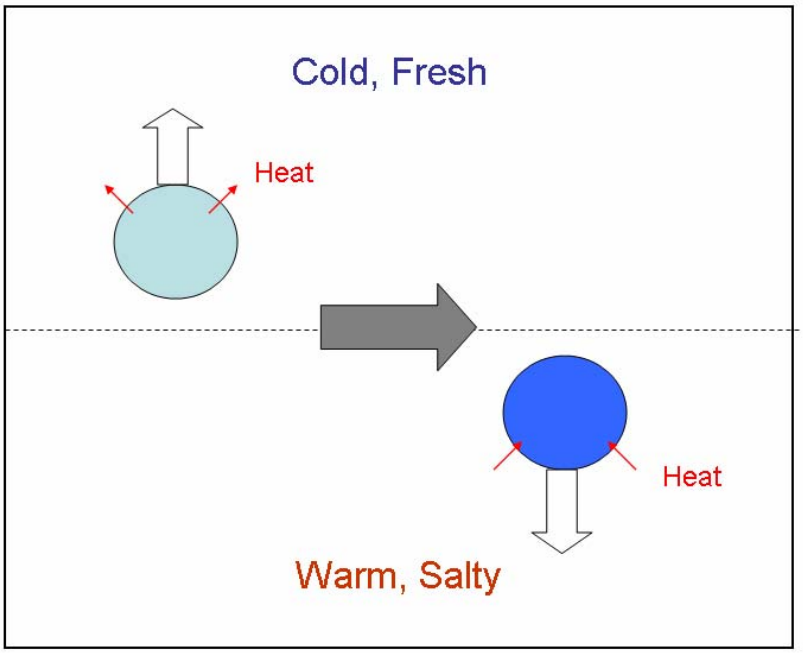

Figure 3. Schematic diagram of oscillatory diffusive convection.

More common in the ocean is the second mode of diffusive convection, known as the diffusive layering. This mode is characterized by well mixed layers separated by sharp, diffusive interfaces. Figure 4 represents a situation where a cold and fresh layer of water rests on the top of the denser warm and salty layer. In this configuration, the heat will diffuse faster than salt, resulting in the downward density flux across the interface. The region directly below (above) the interface becomes denser (lighter). As a result, the top-heavy convection is maintained on both sides of the interface.

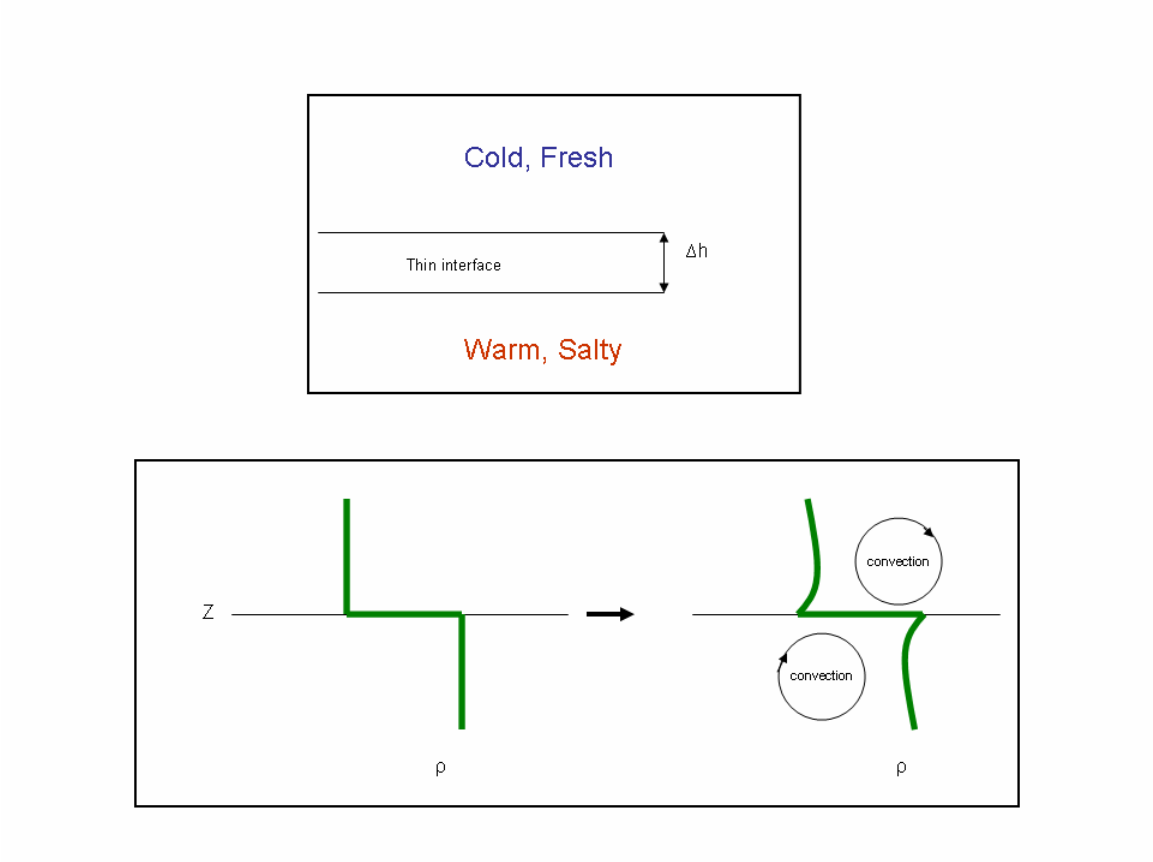

Figure 4. Schematic diagram of diffusive layering.

B. REGIONS SUCEPTABLE TO DOUBLE DIFFUSION

In order to determine which part of the world's oceans will be favorable for double diffusion, two different parameters can be used. Turner (1965) described the dependence of the relative strength of double diffusion on the density ratio as

$$R_\rho = \frac{\alpha T_Z}{\beta S_Z} \qquad (1)$$

where α is the coefficient of thermal expansion, β is the coefficient of saline contraction, and T_Z and S_Z are the

vertical temperature and salinity gradients, respectively. The definition of density ratio (1) is used for the salt finger regime of double diffusion; the diffusive convection is described by the inverse of (1). The most intense double diffusion for both regimes is realized when R_ρ approaches 1. There are associated difficulties with mapping world oceans' favorability to double diffusion based on R_ρ. You (2002) points out that most ocean regions often show extremely large positive or negative values of R_ρ, making the interpretation difficult.

To simplify interpretation, Ruddick (1983) presented the Turner angle, Tu, named in honor of J. Stewart Turner:

$$Tu(\deg) = \tan^{-1}\left(\alpha\frac{\partial T}{\partial z} - \beta\frac{\partial S}{\partial z}, \alpha\frac{\partial T}{\partial z} + \beta\frac{\partial S}{\partial z}\right). \qquad (2)$$

R_ρ and Tu can be related by

$$R_\rho = -\tan(Tu + 45). \qquad (3)$$

The physical meaning of the Turner angle is described in Figure 5. To summarize, when -90 deg <Tu<-45 deg (or $0<R_\rho<1$, as defined in equation (1), diffusive convection is possible; when -45 deg <Tu<45 deg (or $0<R_\rho<\pm\infty$), the water column is stably stratified with respect to T and S, and double diffusion is not possible; and when 45 deg <Tu<90 ($1<R_\rho<\pm\infty$) the salt finger regime can be expected.

You (2002) used the 1994 Levitus climatological atlas to calculate Tu for the world oceans. The three major ocean basins are displayed in Figures 6-8. He notes that about 44%

of the oceans are favorable for double diffusion, of which 30% takes the form of salt fingering, and 14% is diffusively favorable.

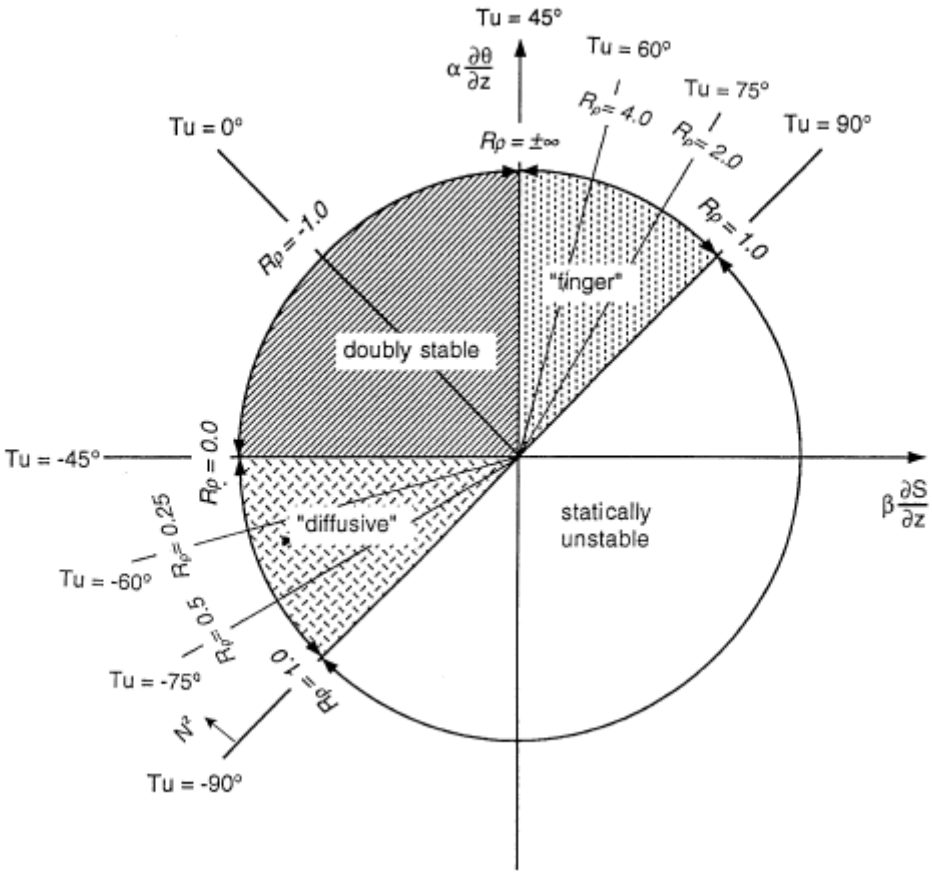

Figure 5. Illustration of Turner angle Tu (degrees)with corresponding R_ρ value indicated. Adopted from You (2002).

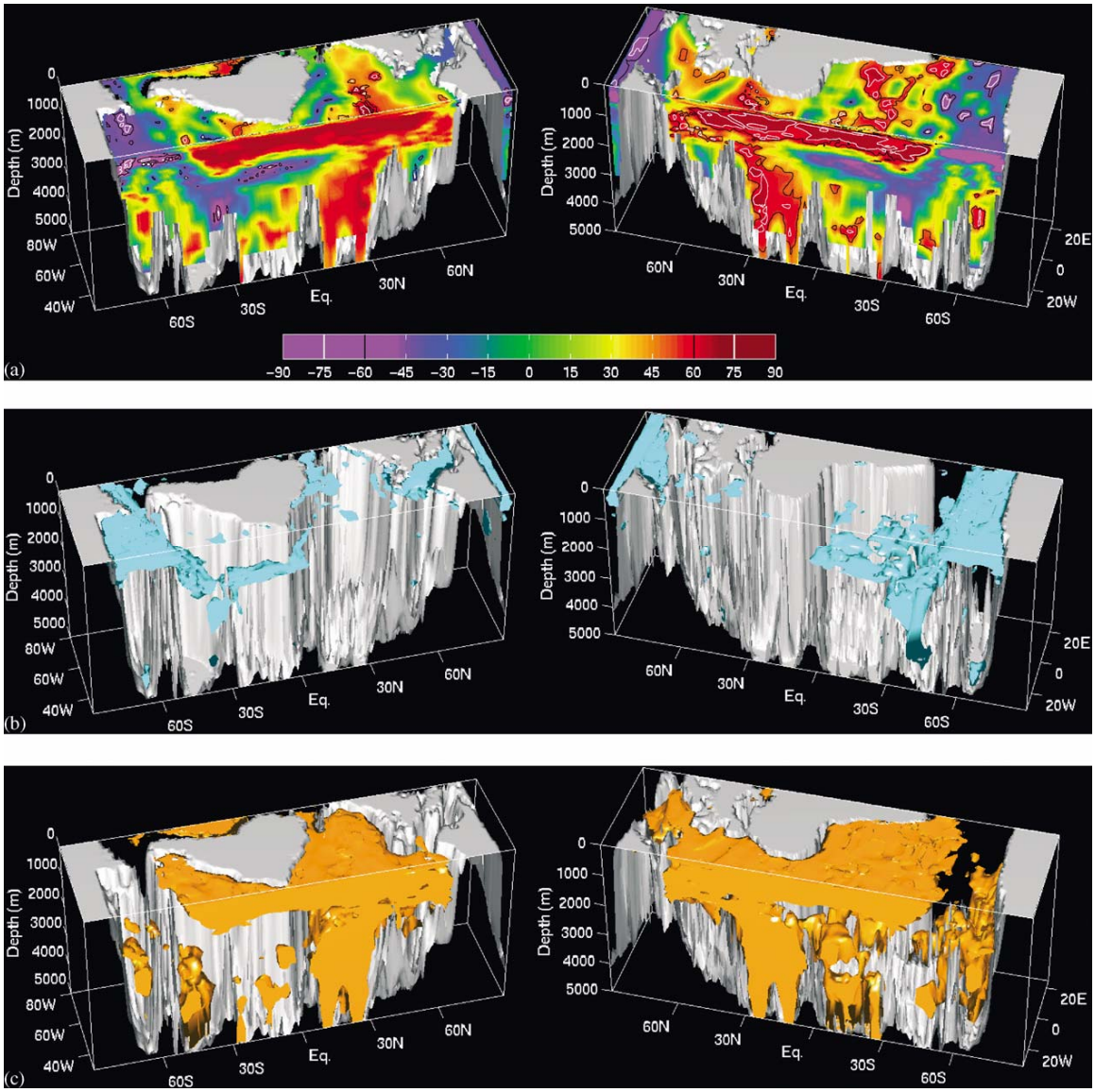

Figure 6. 3D plots of (a) Tu: the color bar marks diffusive convection(-90 deg<Tu<-45 deg), doubly stable (-45 deg<Tu<45 deg), and salt-fingering(45 deg<Tu<90 deg),(b)diffusive convection only and (c)salt-fingering only in the western (left panel) and eastern (right panel) Altantic Ocean. Adopted from You (2002).

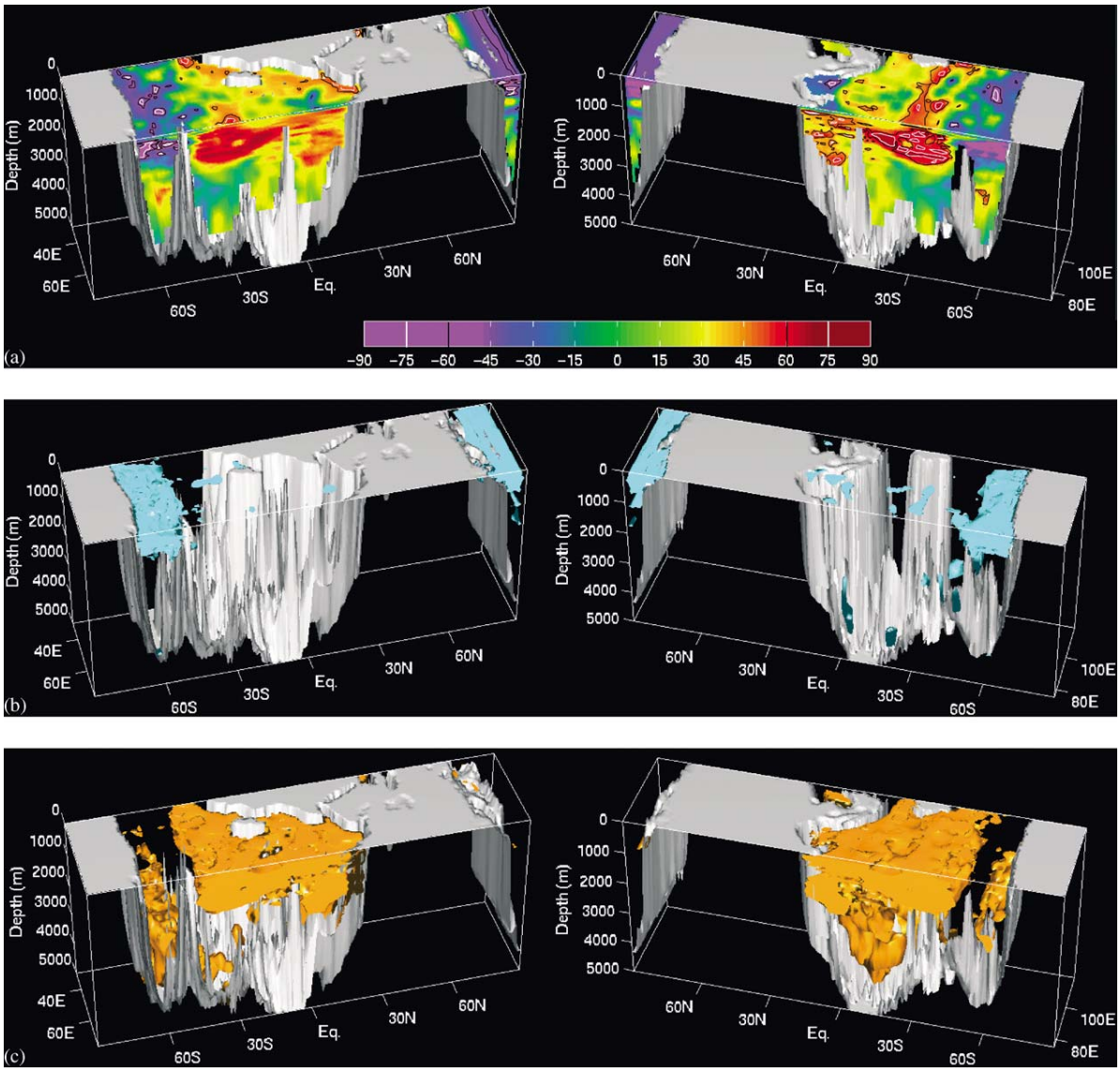

Figure 7. Same as Figure 4, but for Indian Ocean

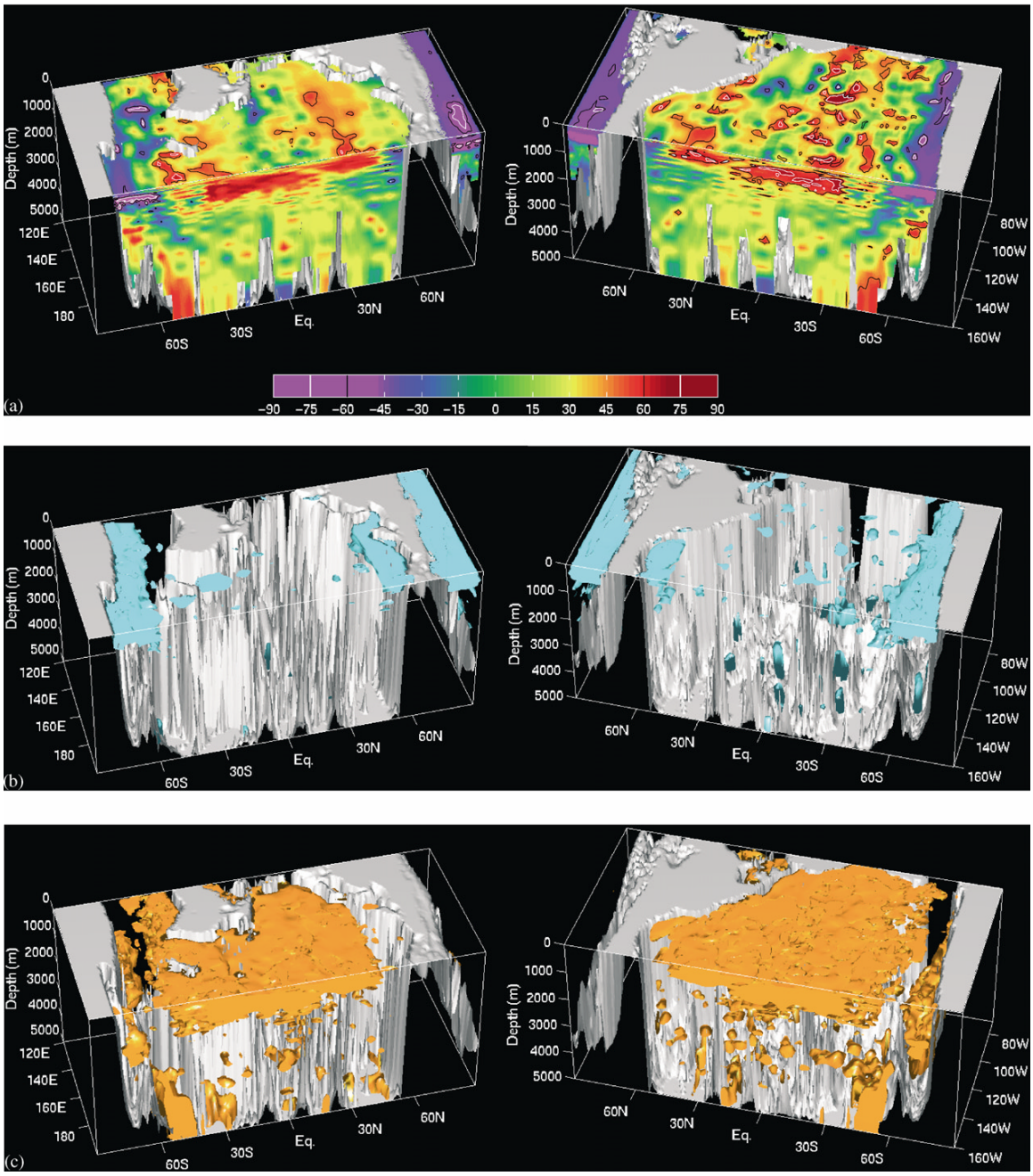

Figure 8. Same as Figure 5, but for the Pacific Ocean.

C. THERMOHALINE STAIRCASES

One of the most fascinating aspects of double-diffusive convection is related to its ability to form stepped structures. These so called thermohaline staircases consist of mixed layers which are separated by thin stratified interfaces. There have been several theories proposed to explain the origin of theromohaline staircases. One of the earliest is the collective instability mechanism (Stern, 1969), which attributes the staircase formation to the interaction between waves and double-diffusion, resulting in a system of sheets and layers; a relatively recent hypothesis that steps in temperature and salinity profiles represent intrusions evolving into a staircase (Merryfield, 2000); and the latest theory proposes that layers form as a result of the instability of the flux gradient laws – the instability which manifests itself in the form of growing, horizontally uniform perturbations transforming the basic gradient into a well-defined thermohaline staircase (Radko, 2003, 2005).

Salt finger staircases are normally observed when R_ρ is less than 2; however, staircases associated with diffusive-convection have been observed over a wider range of $1<R_\rho<10$. Recent field data from the Atlantic Ocean have shown that vertical fluxes within thermohaline staircases are significantly (by an order of magnitude) enhanced over non-staircase regions with similar stratifications (Schmitt et al., 2005). Thus, it is vital to improve our understanding of thermohaline staircase formation, evolution and the large scale consequences. In this study, it is

argued that staircases could have an impact on the oceanic heat budget in the Arctic Ocean.

D. EQUILIBRIUM STRUCTURE OF DIFFUSIVE STAIRCASES

Another interesting feature of diffusive staircases is related to their evolution over time. The layers which form initially are unstable and thin. They merge continuously, which results in increasing step height until an equilibrium thickness is reached. This merging of layers in diffusive staircases is attributed to the secondary instabilities of steady-state staircases (Radko, 2005). Two merging mechanisms are possible: either layers merge when interfaces drift and collide (Balmforth et al., 1998), or the steps with small buoyancy variations become even weaker and eventually vanish (Merryfield, 2000). Radko (2005) observed that formation and equilibration of the staircase increased the diffusive fluxes by almost an order of magnitude.

One of the aims of this study is the evaluation of diffusive fluxes; therefore, it is necessary to introduce the flux law for diffusive convection. The so-called 4/3 flux law for diffusive convection was formulated by Turner (1965). The 4/3 flux law relates temperature flux F_T (in degrees C m $s.^{-1}$) and salinity flux F_s (in m $s.^{-1}$) to the temperature and salinity steps across the diffusive interface (ΔT and ΔS) as follows:

$$\alpha F_T = C(g\kappa_T^2/\nu)^{1/3}(\alpha\Delta T)^{4/3} \qquad (4)$$

$$\beta F_S = \alpha F_T \gamma \qquad (5)$$

where $C(R_\rho)$ and $\gamma(R_\rho)$, k_T is the molecular diffusivity of heat, ν is the kinematic viscosity, g is the gravitational

acceleration, α is the coefficient of thermal expansion, β is the coefficient of haline contraction, γ is the flux ratio, and C is a constant determined from experimental data or oceanic observations assuming that the 4/3 flux law is valid. In (4) and (5), dimensional fluxes are used. The 4/3 flux law is therefore independent of stair thickness, but dependent on the density ratio. Dimensional considerations (Turner, 1973) suggest that both γ and C are uniquely determined by the density ratio, R_ρ.

II. NUMERICAL SIMULATION

A. MODEL DESCRIPTION

In order to study oscillatory diffusive convection, two dimensional numerical simulations were performed on the Naval Postgraduate School High Performance Computing Center Linux clusters. Following Radko & Stern (1999), the temperature and salinity fields were decomposed into the linear basic state ($\overline{T}, \overline{\mathrm{S}}$) and perturbations ($\mathrm{S}, \mathrm{T}$) of it. For computational convenience, Boussinesq equations were non-dimensionalized. Therefore, $\mathrm{d}=(\mathrm{k_T}\nu/\mathrm{g}\alpha\overline{T}_z)^{1/4}$ represents the unit of length, $\mathrm{k_T}/\mathrm{d}$ is the velocity scale, $\mathrm{d}^2/\mathrm{k_T}$ represents the time scale, $\mathrm{k_T}$ is the molecular diffusivity of heat, ν is the kinematic viscosity, g is the gravitational acceleration, α is the coefficient of thermal expansion and $\overline{\mathrm{T}_z}$ is the temperature gradient. Wilson (2007) computed $\overline{\mathrm{T}_z}$=0.015 based on the average 1.5 deg C decrease in T over 100 m depth in the diffusive layer in the Beaufort Gyre. Similarly, $\alpha \mathrm{T}_z d$ is the scale for both temperature and salinity perturbations, resulting in

$$\left.\begin{aligned} &\frac{1}{\mathrm{Pr}}\frac{dv}{dt} = -\nabla p + \nabla^2 v + (T-S)k, \\ &\nabla \cdot v = 0, \\ &\frac{dT}{dt} - w = \nabla^2 T, \\ &\frac{dS}{dt} - \frac{1}{R_0} w = \tau \nabla^2 S, \end{aligned}\right\} \qquad (6)$$

where $\mathrm{Pr} = \nu/\mathrm{k_T}$ is the Prandtl number, $\tau = \mathrm{k_S}/\mathrm{k_T}$ is the molecular diffusivity ratio (Lewis number), R_ρ is the density ratio for the basic uniform S – T gradient, and v, T, S are non-dimensional velocity, temperature, and salinity. For parameters of Arctic staircases, $d \approx 1$ cm, $t \approx 686$ seconds.

The conversion formula for temperature flux is

$$F_{Tdim} = F_{Tnon\text{-}dim}\ \kappa_T\, dT/dz \qquad (7)$$

and the corresponding heat flux is

$$F_{Hdim}\ (W\ m^{-2}) = F_{Tdim}\ (m/s\ K) C_p\ \rho \qquad (8)$$

where C_p is the specific heat for sea water and ρ is the density of sea water. Substituting (7) into (8) yields the conversion factor of 0.0084.

Unless specified otherwise, the diffusivity ratio of $\tau = 1/10$ was used, which is an order of magnitude greater than the true value for heat/salt ($\tau = 1/100$). This greater value was selected purely for numerical convenience. Numerical calculations with a true diffusivity ratio would require resolving the extremely fine salt dissipation scale, which is by far less than the characteristic size of the diffusive layers, and the calculations would be computationally prohibitive. As was pointed out in Stern et al.,(2001), such a modification is not expected to alter the fundamental physics and dynamics of the diffusive convection. Furthermore, a simple extrapolation procedure is be used to evaluate the heat/salt ($\tau = 0.01$) fluxes from $\tau = 0.1$ numerical simulations.

A fully dealiased pseudospectral method described and first used in Stern & Radko(1998) is employed to obtain a two dimensional numerical solution for the system of equations (6) above. The solution is doubly-periodic in x and z. All numerical algorithms were coded in Fortran.

B. PRELIMINARY CALCULATIONS

In order to gain confidence in the numerical calculations, and to better understand the dynamics of the diffusive convection, a simple experiment was carried out initially. The experiment was initiated from a random computer-generated distribution of T and S and is shown in Figures 9 and 10. This experiment was performed using a uniform grid of 512x1024 nodes and non-dimensional grid spacing delta x=y=0.75 which corresponds to a vertical scale of 7.5 m, and R_ρ = 1.1. The first stage of the experiment (t<50) is characterized by the development of small scale diffusive plumes presented in Figure 9. At t=500, the field of diffusive plumes arranged itself into a system of well defined horizontal steps. Next, a series of merging events occurred: between t= 500 and t=600 the number of steps decreased from 9 to 6 as shown in Figures 9 and 10. Six steps merged into three in less than 100 time units, or approximately 19 hours. The experiment reached the equilibrium at approximately t=800 when the staircase evolved into two final steps, as shown in Figure 11. The equilibrium step height in the final stage was 3.75 m. The experiment was continued until t=950; however, no merging took place during this period.

The time series of fluxes for this experiment, which are computed over the whole computational domain, is shown in Figure 12. It confirms that the diffusive fluxes increase with each merging event, and once the equilibrium thickness of the steps is reached, the fluxes decrease by about half of their value and, subsequently, remain roughly constant.

This preliminary numerical experiment indicates:

(i) sensitivity of fluxes to the step size

(ii) the tendency of the weak steps to merge

The mechanics of merging in a staircase and associated fluxes are now analyzed in greater detail.

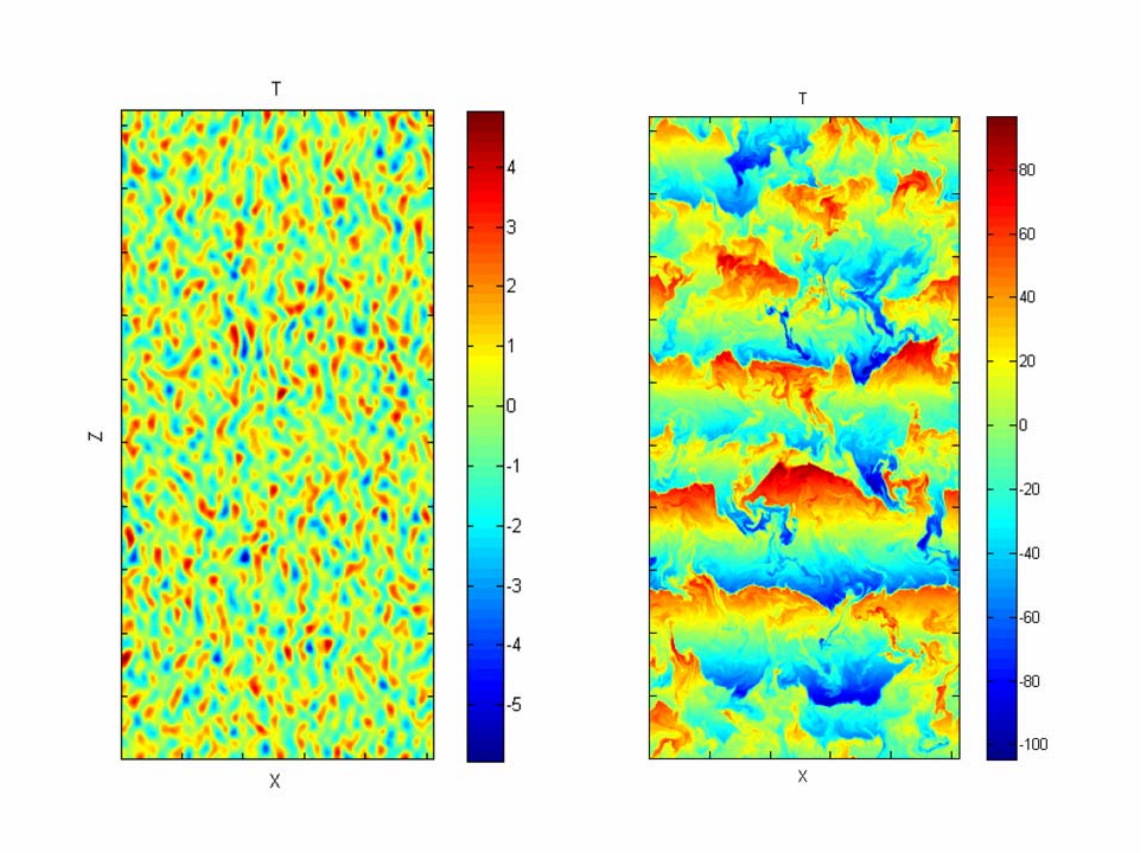

Figure 9. Formation of layers in a double-diffusive numerical experiment. The left figure shows a well developed field of two dimensional diffusive plumes after t=50. Note the well defined horizontal layers in the right figure after t=500. The red color corresponds to high values of T; the low values are shown in blue.

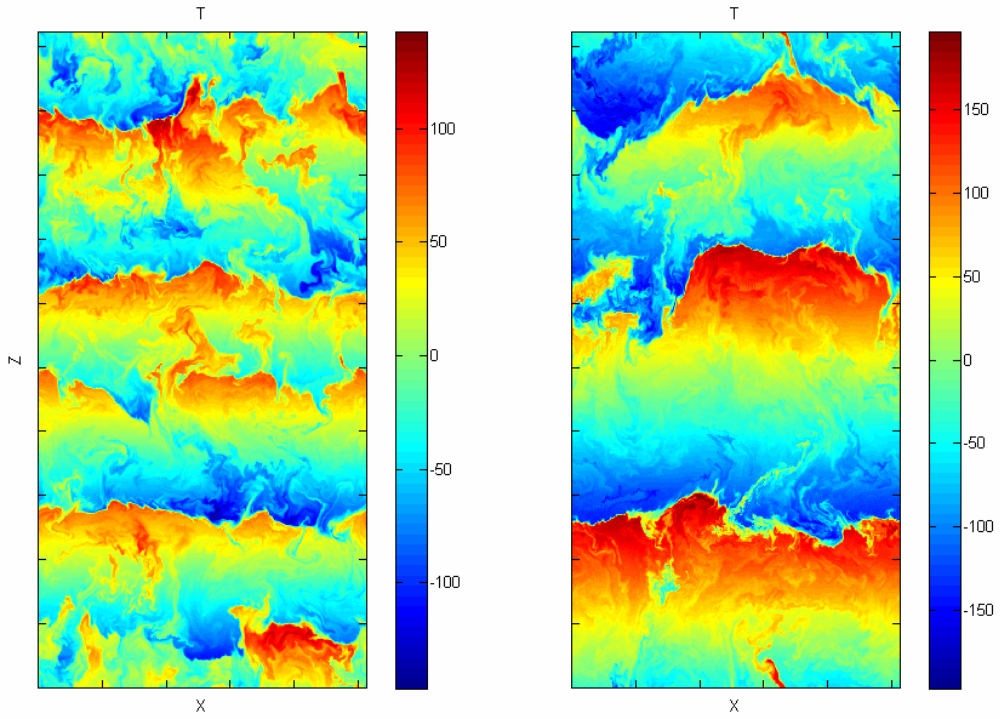

Figure 10. Continuation of the numerical experiment from Figure 9 demonstrates merging of diffusive layers. Note six layers in the left figure at t=600 merging into four layers at t=700.

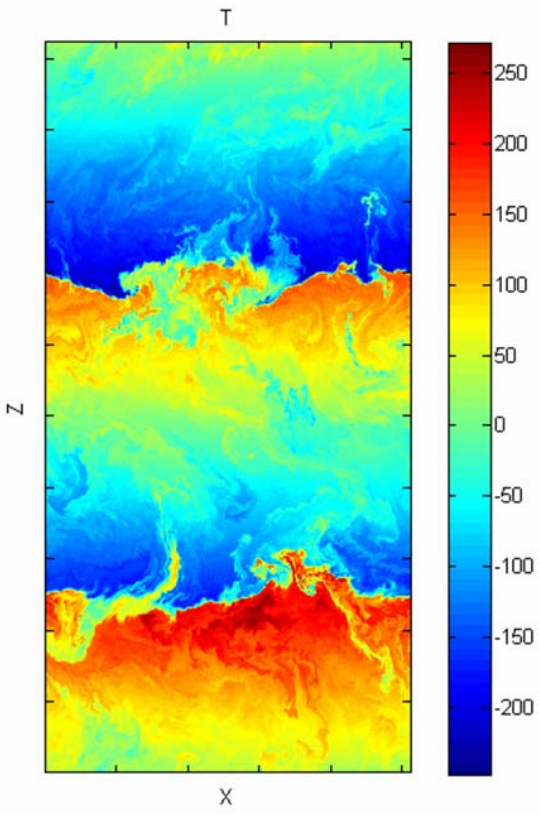

Figure 11. Continuation of the numerical experiment from Figures 9 and 10. The equilibrium state shows 2 layers.

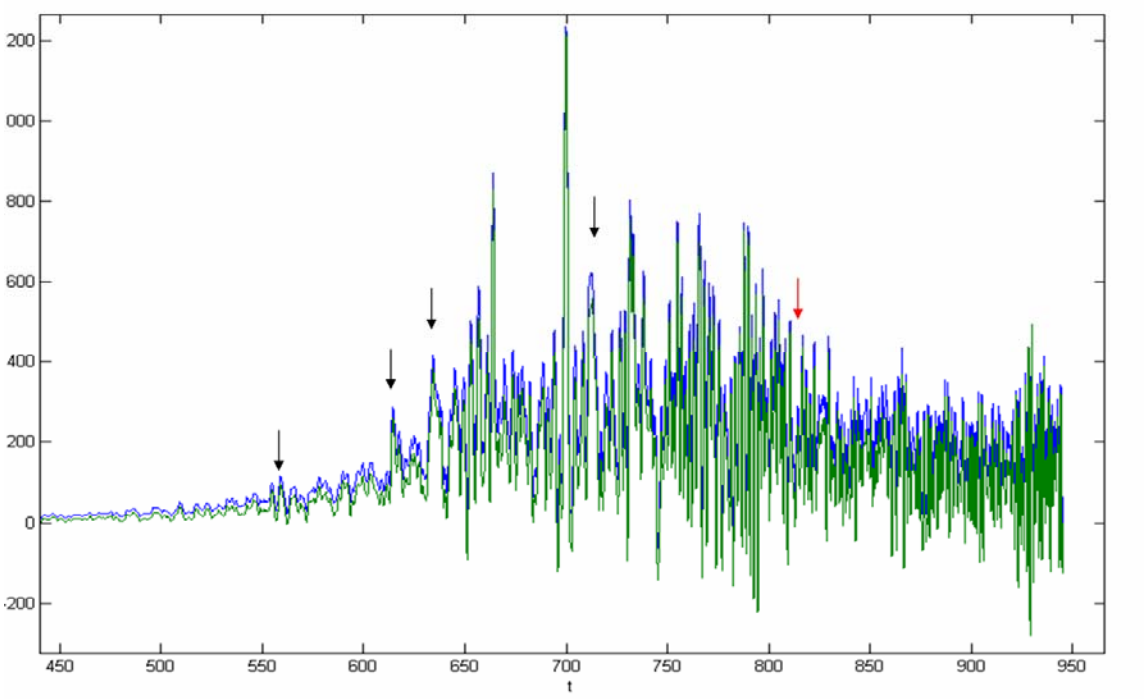

Figure 12. Time series of diffusive fluxes in the numerical experiment initiated from random noise. The blue curve indicates heat flux, the green one salinity flux. The arrows indicate a merging event, the red arrow an equilibrium state.

C ONE-STEP FLUXES

Turner (1973) extensively discussed the diffusive instability. One of the most important properties of well formed diffusive interfaces is the temperature and salinity flux across them. Padman (1994) and Muench et al (1990) indicated that diffusive convection could be a significant process influencing the vertical fluxes of heat and salt from the warm and salty intermediate water upwards to the polar mixed layers and sea ice. The basin-averaged estimate of heat loss from the Atlantic layer is 7 W m^{-2}(Aagaard and Greisman, 1975). Previous studies (Padman et al., 1987) estimated heat flux using the extrapolation of the

laboratory flux laws to the ocean and reported values of 0.02 to 0.1 W m^{-2}. However, based on the analysis of the Arctic thermohaline staircase from the Beaufort Gyre experiment, Wilson (2007) reported that the diffusive fluxes could be an order of magnitude greater than the diffusive fluxes determined from previous laboratory experiments. Use of the direct numerical simulations opens a possibility for resolving the controversy with regard to the magnitude of diffusive fluxes.

A series of one-step numerical experiments was performed in order to determine the magnitude of diffusive fluxes numerically and compare them with those from the laboratory and field observations. The range of R_ρ was from 1.1 to 5.0. The upper range of the values of R_ρ is more significant for the comparison with the Wilson (2007) Arctic Ocean results, since the values of R_ρ in the thermohaline staircases in that geographic region are 5 or higher. The vertical scale of steps was varied as well, in order to examine dependencies of simulated fluxes and structures on H. The step thicknesses were varied from 0.75 to 3 m and the results are summarized in Table 1.

As expected, the fluxes generally decrease with increasing R_ρ. The fluxes also generally increase with increasing layer thickness, H, except for a few values in the range of R_ρ<1.9 and H>3.0m. However, these differences are small and can be attributed to the incomplete equilibration in some runs.

Layer Thickness (m)	R_ρ									
	1.1	1.3	1.5	1.7	1.9	2.1	2.3	3.0	4.0	5.0
0.75	62.8	28.9	20.9	13.1	9.13	6.90	4.94	3.08	1.95	1.24
1.5	155	58.2	43.1	33.2	24.9	20.5	20.8	11.8	9.27	7.76
3.0	45.9	49.2	31.3	30.3	26.5	18.0	19.0	14.1	11.3	10.3

Table 1. Diffusive heat flux (non-dimensional) as the function of density ratio and layer thickness.

D MERGING EVENTS

Next, in order to better understand the mechanics of merging in a staircase (see Figures 9, 10), several numerical experiments were performed to isolate the merging process. The initial setup consisted of two almost identical steps; the focus was on the evolutionary pattern and the time scale of expected merging events. All experiments were initiated in the mesh grid of 512 x 512 points and delta x=y=0.3 which corresponded to a vertical scale of 1.5 m. The value of R_ρ was varied from 1.2 to 1.5. For each experiment, the value of R_ρ was slightly higher for one interface and slightly lower for the other. The representative numerical experiment in this series is shown in Figures 13-15. After approximately t=100, the erosion of one of the steps is noticeable in Figure 13. The process continues until the step is completely eroded at t=400.

Figures 14 and 15 illustrate a gradual weakening of the interface until its complete disappearance at t=400,

indicating that a merging event took place between t=300 and t=400. Visual inspection of the evolutionary pattern indicates that the interfaces remains stationary and the weaker one is gradually eroded until it completely disappears.

Figure 16 represents a time series of numerical fluxes for the same two-step experiment. Note the increase in the fluxes indicating the merging of two steps into one. The jump in fluxes occurs at t=350, indicating the exact time the merging event took place. This coincides with findings from Figures 13-15.

The experiments are summarized in Table 2. The results confirm that with increasing R_ρ, the diffusive fluxes decrease. Each experiment exhibits a rough doubling of fluxes once merging takes place. The time scale of merging increases with increasing R_ρ. The numerical results will be explored further once the theoretical framework for understanding merging events – the merging theorem – is developed in Chapter III.

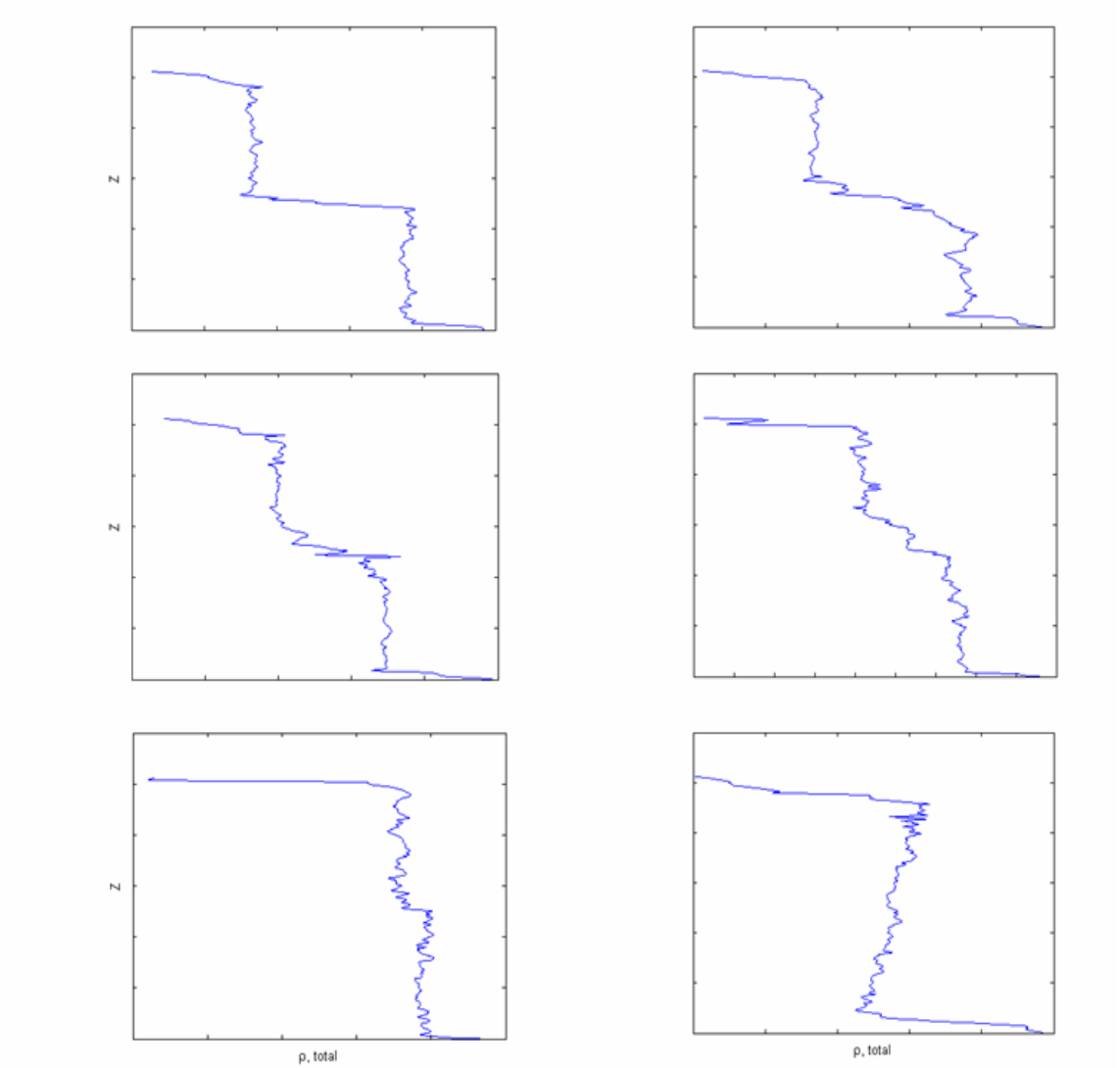

Figure 13. Numerical experiment showing merging evolution of two steps into one. The plots show the total averaged density for the simulation, from left to right at t=25,100,200,300,350,400. The initial step height in the experiment is 0.75 meters.

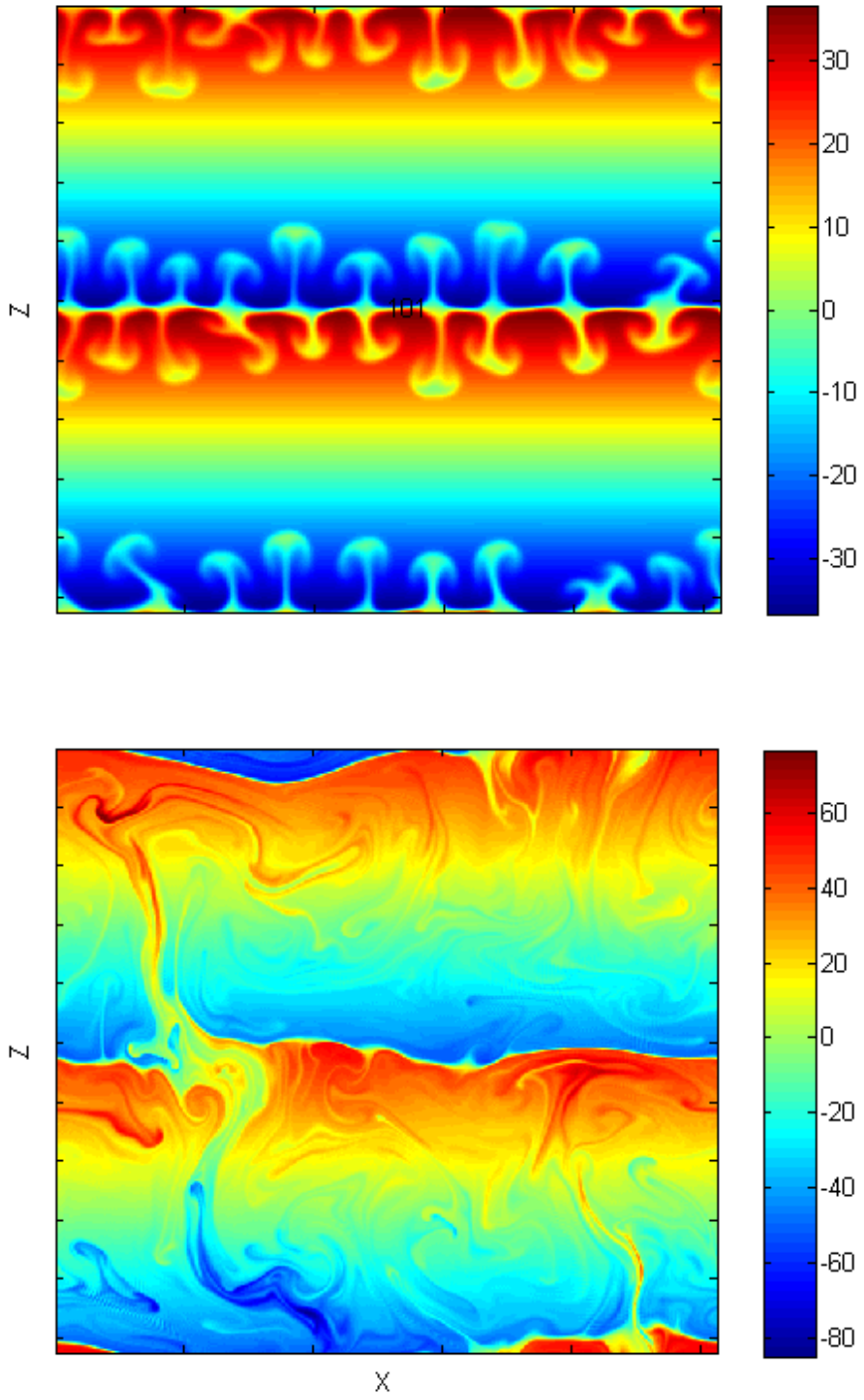

Figure 14. Evolution of merging event in a numerical experiment of a two-step system. The top figure shows a sharp interface and clearly formed diffusive plumes.

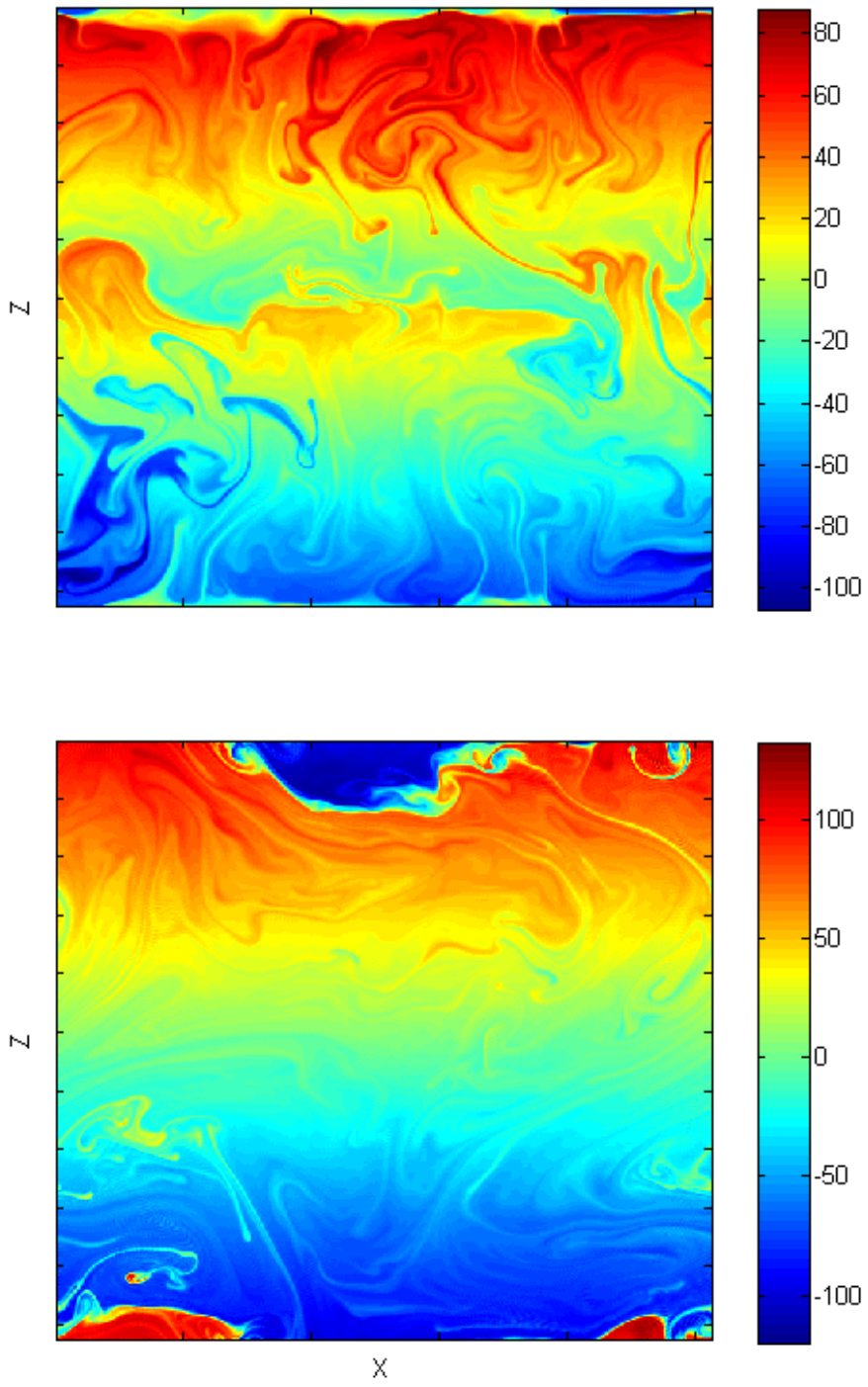

Figure 15. Continuation of merging experiment. The top figure shows weak interface at t=300. In the bottom figure, the middle interface is no longer present at t=400.

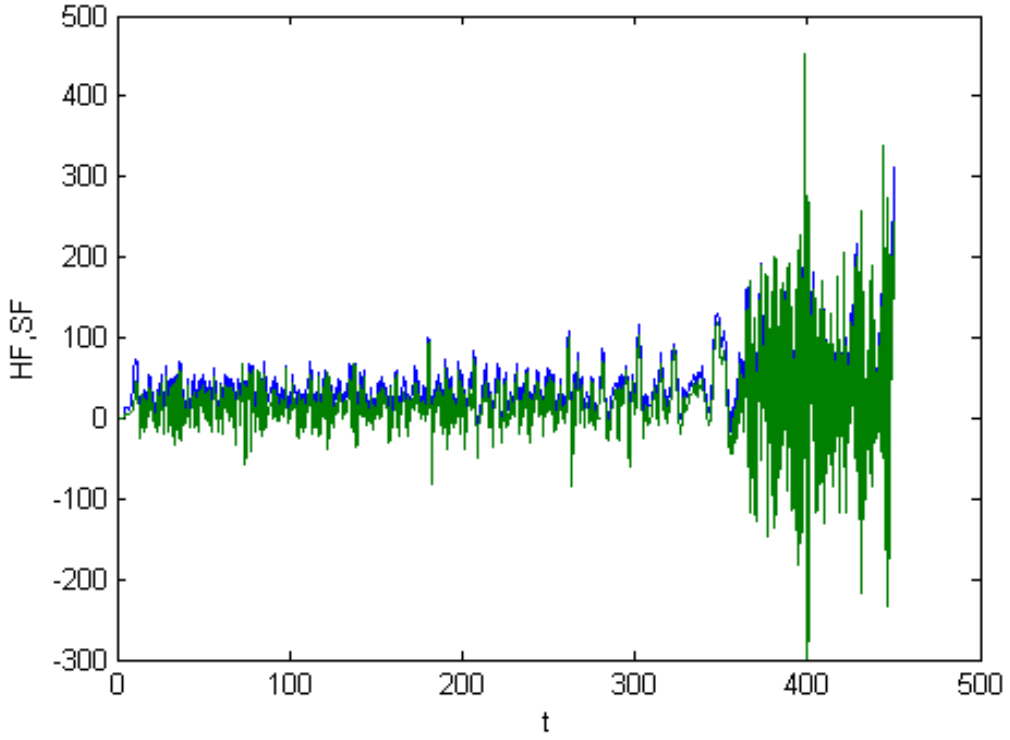

Figure 16. Time series of diffusive fluxes in a two-step numerical experiment. The blue curve represents heat flux; the green one represents salinity.

R_ρ	$\overline{F_T}$ before merging	$\overline{F_T}$ after merging	Time (non-dim.)
1.2	48	119	130
1.3	41	83	350
1.4	31	70	950

Table 2. Summary of two-step numerical experiments.

THIS PAGE INTENTIONALLY LEFT BLANK

III. MERGING THEOREM

A. INTRODUCTION

The existence of thermohaline staircases in the ocean has been well established (Kelley, 1984; Schmitt, 1994). They frequently occur in the ocean regions where the conditions for double diffusive instability are favorable. The mechanics proposed for their origin and evolution have been discussed in the Introduction. Here, the mechanism for the merging of such staircases will be explored and subsequently tested in a series of numerical experiments.

Two mechanisms for the merging of staircases have been studied: either layers merge when interfaces drift and collide, or the interfaces will erode over time without exhibiting any vertical motion. The first mechanism has been proposed by Balmforth et al (1998) who formulated a one-dimensional model of the mechanically forced turbulence in a stratified fluid. Following Radko (2007), this mechanism will be referred to as H-merger. The second mechanism, which was described by Merryfield (2000), who modeled the up gradient buoyancy flux in a double-diffusion favorable fluid. According to his model, the steps with small buoyancy variations weaken even further and eventually vanish. Again, following Radko (2007), this mechanism will be referred to as B-merger.

This chapter is organized as follows: First, the merging theorem for the two-component H- and B- merger will be formulated. Next, a physical explanation of B- merger will be presented, and the relationship between the density

ratio, R_ρ, and the diffusivity ratio, γ, will be demonstrated. Lastly, the relationship between the mechanics of merging and the variation in the diffusivity ratio will be explored.

The starting point for the derivation of the two component merging theorem is the two component buoyancy conservation equation where T(z,t) and S(z,t) are heat and salinity, respectively. F^T and F^S are heat and salinity fluxes, respectively.

$$\left.\begin{aligned} \frac{dT}{dt} &= \frac{dF^S}{dz} \\ \frac{dS}{dt} &= \frac{dF^T}{dz} \end{aligned}\right\} \qquad (9)$$

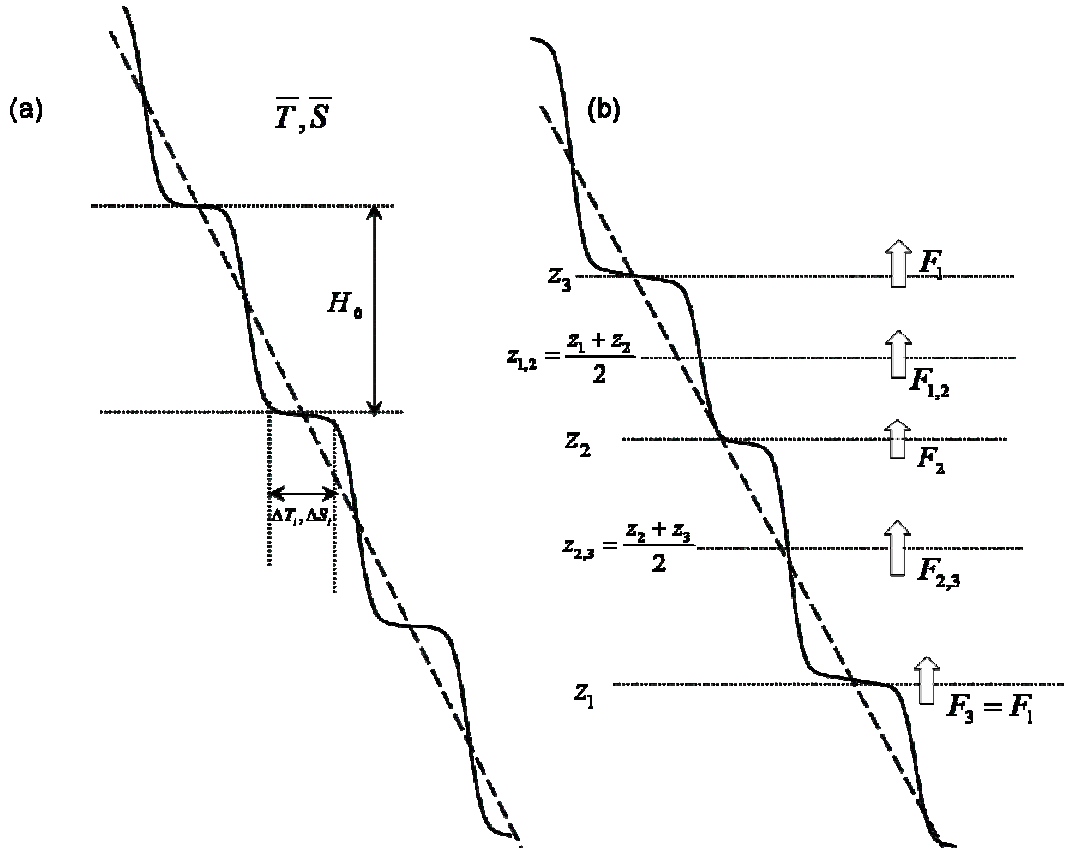

Figure 17. Schematic representation of the stability analysis for a periodic system of layers and interfaces. (a) Basic state with equal steps. (b) Perturbed state with the slightly increased buoyancy jumps at even interfaces and with the correspondingly decreased jumps at odd interfaces.

Following Radko's (2007) one-component theory, we express the heat (T) and salinity (S) variations across a two step system in Figure 17(b) as follows:

$$\left.\begin{aligned} T_{12}-T_{01} &= T-\delta \\ T_{23}-T_{12} &= T+\delta \\ S_{12}-S_{01} &= S-\varepsilon \\ S_{23}-S_{12} &= S+\varepsilon, \qquad (\delta,\varepsilon) << (T,S) \end{aligned}\right\} \tag{10}$$

where $T = (\partial\overline{T}/\partial z)H$ and $S = (\partial\overline{S}/\partial z)H$ are the temperature and salinity variation across one step in Figure 17(a), respectively. Symbols δ and ε represent a small perturbation to T and S, respectively. Note that the thicknesses of two layers in Figure 17 (b) are not necessarily equal:

$$\left.\begin{aligned} H_{1,2} &= H - h \\ H_{2,3} &= H + h, \qquad h << H \end{aligned}\right\} \tag{11}$$

where H_{nn+1} represents the distance between the two interfaces $z = z_n$ and $z = z_{n+1}$. For convenience, the buoyancy equation is expressed in the integral form, which is accomplished by integrating (9) over the interval$[z_{bot}, z_{top}]$:

$$\left.\begin{aligned} \int_{z_{bot}}^{z_{top}} \frac{\partial T}{\partial t} dz &= \int_{z_{bot}}^{z_{top}} \frac{\partial F^T}{\partial t} dz = F^T(z_{top}) - F^T(z_{bot}) \\ \int_{z_{bot}}^{z_{top}} \frac{\partial S}{\partial t} dz &= \int_{z_{bot}}^{z_{top}} \frac{\partial F^S}{\partial t} dz = F^S(z_{top}) - F^S(z_{bot}) \end{aligned}\right\} \tag{12}$$

where two levels $z_{top}(t)$ and $z_{bot}(t)$ can vary in time. Utilizing the identity

$$\left.\begin{aligned} \frac{d}{dt}\int_{z_{bot}}^{z_{top}} T dz &= \int_{z_{bot}}^{z_{top}} \frac{\partial T}{\partial t} dz + \frac{dz_{top}}{dt} T(z_{top}) - \frac{dz_{bot}}{dt} T(z_{bot}) \\ \frac{d}{dt}\int_{z_{bot}}^{z_{top}} S dz &= \int_{z_{bot}}^{z_{top}} \frac{\partial S}{\partial t} dz + \frac{dz_{top}}{dt} S(z_{top}) - \frac{dz_{bot}}{dt} S(z_{bot}) \end{aligned}\right\} \tag{13}$$

the equation (13) is re-written to a new form

$$\left.\begin{aligned} \frac{d}{dt}\int_{z_{bot}}^{z_{top}} T dz &= \frac{dz_{top}}{dt} T(z_{top}) - \frac{dz_{bot}}{dt} T(z_{bot}) + F^T(z_{top}) - F^T(z_{bot}) \\ \frac{d}{dt}\int_{z_{bot}}^{z_{top}} S dz &= \frac{dz_{top}}{dt} S(z_{top}) - \frac{dz_{bot}}{dt} S(z_{bot}) + F^S(z_{top}) - F^S(z_{bot}) \end{aligned}\right\}. \tag{14}$$

Next, the integral relation in (14) is applied to the individual layers $[z_n, z_{n+1}]$ resulting in

$$\left.\begin{aligned} \frac{d}{dt}\int_{z_n}^{z_{n+1}} T dz &= \frac{dz_{n+1}}{dt}T_{n+1} - \frac{dz_n}{dt}T_n + F_n^T - F_{n+1}^T \\ \frac{d}{dt}\int_{z_n}^{z_{n+1}} S dz &= \frac{dz_{n+1}}{dt}S_{n+1} - \frac{dz_n}{dt}S_n + F_n^S - F_{n+1}^S \end{aligned}\right\} \qquad (15)$$

where $F_i=F(z_i)$. The greatest contribution to the integrals of temperature and salinity in equation (15) comes from the interior of layers where the gradients of temperature and salinity are nearly uniform, and therefore

$$\left.\begin{aligned} \int_{z_n}^{z_{n+1}} T dz &\approx T_{n\,n+1} H_{n\,n+1} \\ \int_{z_n}^{z_{n+1}} S dz &\approx S_{n\,n+1} H_{n\,n+1} \end{aligned}\right\}. \qquad (16)$$

Applying equations (15) and (16)to two successive layers $[z_n, z_{n+1}]$ where n = 1,2 yields

$$\left.\begin{aligned} \frac{d}{dt}\left(H_{12}T_{12}\right) &= F_2^T - F_1^T \\ \frac{d}{dt}\left(H_{23}T_{23}\right) &= F_3^T - F_2^T \\ \frac{d}{dt}\left(H_{12}S_{12}\right) &= F_2^S - F_1^S \\ \frac{d}{dt}\left(H_{23}S_{23}\right) &= F_3^S - F_2^S . \end{aligned}\right\} \qquad (17)$$

Due to a substantial variation in temperature and salinity across the interfaces, it is essential to define the temperature and salinity at the interface T_n, S_n. The center of the interface is defined as a point where the temperature

and salinity are average values at the center of the two neighboring layers

$$\left.\begin{aligned} T_n &= \frac{T_{n-1n} + T_{nn+1}}{2} \\ S_n &= \frac{S_{n-1n} + S_{nn+1}}{2} \end{aligned}\right\}. \qquad (18)$$

A similar set of integral equations results from the temperature and salinity budgets for areas enclosed by the centers of the neighboring layers $[z_{nn+1}]$:

$$\left.\begin{aligned} \frac{d}{dt}\left(\frac{H_{12}T_{12}}{2} + \frac{H_{23}T_{23}}{2} + \frac{H_{12}\Delta T_{L12}}{8} - \frac{H_{23}\Delta T_{L23}}{8}\right) &= \frac{dz_{23}}{dt}T_{23} - \frac{dz_{12}}{dt}T_{12} + F_{23}^{T} - F_{12}^{T} \\ \frac{d}{dt}\left(\frac{H_{23}T_{23}}{2} + \frac{H_{34}T_{34}}{2} + \frac{H_{23}\Delta T_{L23}}{8} - \frac{H_{34}\Delta T_{L34}}{8}\right) &= \frac{dz_{34}}{dt}T_{34} - \frac{dz_{23}}{dt}T_{23} + F_{34}^{T} - F_{23}^{T} \\ \frac{d}{dt}\left(\frac{H_{12}S_{12}}{2} + \frac{H_{23}S_{23}}{2} + \frac{H_{12}\Delta S_{L12}}{8} - \frac{H_{23}\Delta S_{L23}}{8}\right) &= \frac{dz_{23}}{dt}S_{23} - \frac{dz_{12}}{dt}S_{12} + F_{23}^{S} - F_{12}^{S} \\ \frac{d}{dt}\left(\frac{H_{23}S_{23}}{2} + \frac{H_{34}S_{34}}{2} + \frac{H_{23}\Delta S_{L23}}{8} - \frac{H_{34}\Delta S_{L34}}{8}\right) &= \frac{dz_{34}}{dt}S_{34} - \frac{dz_{23}}{dt}S_{23} + F_{34}^{S} - F_{23}^{S} \end{aligned}\right\} \qquad (19)$$

where $F_{nn+1} = F(z_{nn+1})$; $(\Delta T, \Delta S)_{L12}$ and $(\Delta T, \Delta S)_{L23}$ are the temperature and salinity variations across the interior of the layers in Figure 17(b). To formulate the equations for evolution of $\delta, \varepsilon,$ and h in time, the equations (17) and (19) are utilized and the result is simplified using periodicity conditions, yielding:

$$\left.\begin{aligned} H\frac{d\delta}{dt} + 2h\frac{dT_2}{dt} &= -2(F_2^T - F_1^T) \\ H\frac{d\varepsilon}{dt} + 2h\frac{dS_2}{dt} &= -2(F_2^S - F_1^S) \end{aligned}\right\}. \qquad (20)$$

Since it is assumed that the perturbations are relatively small when compared to the basic state, (20) is linearized: We neglect the nonlinear terms $h(dT_2/dt)$ and $h(dS_2/dt)$ in

(20), further reducing(20) to

$$\left.\begin{aligned}\frac{d}{dt}\delta &= -\frac{2}{H}\left(F_2^T - F_1^T\right)\\ \frac{d}{dt}\varepsilon &= -\frac{2}{H}\left(F_2^S - F_1^S\right)\end{aligned}\right\}. \qquad (21)$$

Next, the two equations in (19) are subtracted and after simplifying using the periodicity conditions, the following is obtained:

$$\left.\begin{aligned}T\frac{dh}{dt} - \frac{\Delta T_{L12} + \Delta T_{L23}}{4}\frac{dh}{dt} - \frac{H}{4}\frac{d}{dt}(\Delta T_{L23} - \Delta T_{L12}) &= 2(F_{23}^T - F_{12}^T) + 2\frac{dz_{12}}{dt}\varepsilon,\\ S\frac{dh}{dt} - \frac{\Delta S_{L12} + \Delta S_{L23}}{4}\frac{dh}{dt} - \frac{H}{4}\frac{d}{dt}(\Delta S_{L23} - \Delta S_{L12}) &= 2(F_{23}^S - F_{12}^S) + 2\frac{dz_{12}}{dt}\delta,\end{aligned}\right\}. \qquad (22)$$

Equation (22) is linearized about the steady state in Figure 17. Since $dz_{12}/dt = 0$ in basic steady state, terms $\frac{dz_{12}}{dt}\varepsilon$ and $\frac{dz_{12}}{dt}\delta$ approach zero in the limit of a weak perturbation. It is reasonable then to neglect the non-linear term $2(dz_{12}/dt)$. Realizing that $(\Delta T, \Delta S)_{L12} \approx (\Delta T, \Delta S)_{L23} \approx (\Delta T, \Delta S)_L$, the h-equation is reduced to

$$\left.\begin{aligned}\left(T - \frac{\Delta T_L}{2}\right)\frac{dh}{dt} - \frac{H}{4}\frac{d}{dt}\left(\Delta T_{L23} - \Delta T_{L12}\right) &= 2\left(F_{23}^T - F_{12}^T\right)\\ \left(S - \frac{\Delta S_L}{2}\right)\frac{dh}{dt} - \frac{H}{4}\frac{d}{dt}\left(\Delta S_{L23} - \Delta S_{L12}\right) &= 2\left(F_{23}^S - F_{12}^S\right).\end{aligned}\right\}. \qquad (23)$$

Replacing the instantaneous fluxes in layers and interfaces F_n^T and F_n^S in (21) by the steady one-step fluxes F^T and F^S (Radko 2007) based on the parameters of a region

extending between the centers of two adjacent layers (z_{n-1n} and z_{nn-1}), we arrive at:

$$\left.\begin{aligned} F_1^T &\approx \tilde{F}^T\left(T_{12}-T_{01}, S_{12}-S_{01}, z_{12}-z_{01}\right) \\ F_2^T &\approx \tilde{F}^T\left(T_{23}-T_{12}, S_{23}-S_{12}, z_{23}-z_{12}\right) \\ F_1^S &\approx \tilde{F}^S\left(T_{12}-T_{01}, S_{12}-S_{01}, z_{12}-z_{01}\right) \\ F_2^S &\approx \tilde{F}^S\left(T_{12}-T_{01}, S_{12}-S_{01}, z_{12}-z_{01}\right), \end{aligned}\right\}. \qquad (24)$$

Next, the difference between the temperature and salinity fluxes at the adjacent interfaces is reduced to

$$\left.\begin{aligned} F_2^T - F_1^T &= 2\delta\frac{\partial\tilde{F}^T}{\partial\tilde{T}} + 2\varepsilon\frac{\partial\tilde{F}^T}{\partial\tilde{S}} \\ F_2^S - F_1^S &= 2\delta\frac{\partial\tilde{F}^S}{\partial\tilde{T}} + 2\varepsilon\frac{\partial\tilde{F}^S}{\partial\tilde{S}} \end{aligned}\right\} \qquad (25)$$

and (25) becomes

$$\left.\begin{aligned} \frac{d}{dt}\delta &= -\frac{4\delta}{H}\frac{\partial\tilde{F}^T}{\partial\tilde{T}} - \frac{4\varepsilon}{H}\frac{\partial\tilde{F}^T}{\partial\tilde{S}} \\ \frac{d}{dt}\varepsilon &= -\frac{4\delta}{H}\frac{\partial\tilde{F}^S}{\partial\tilde{T}} - \frac{4\varepsilon}{H}\frac{\partial\tilde{F}^S}{\partial\tilde{S}} \end{aligned}\right\} \qquad (26)$$

1. H – Merger

The fluxes at the center of each layer $F_{n\,n+1}$ are approximated by their corresponding one step layer based on the thickness and buoyancy variation across this layer

$$\left.\begin{aligned} F_{12}^T &= \tilde{F}^T(T_2-T_1, S_2-S_1, z_2-z_1) \\ F_{23}^T &= \tilde{F}^T(T_3-T_2, S_3-S_2, z_3-z_2) \\ F_{12}^S &= \tilde{F}^S(T_2-T_1, S_2-S_1, z_2-z_1) \\ F_{23}^S &= \tilde{F}^S(T_3-T_2, S_3-S_2, z_3-z_2) \end{aligned}\right\} \qquad (27)$$

$$\left.\begin{aligned}\left(T-\frac{\Delta T_L}{2}\right)\frac{dh}{dt}-\frac{H}{4}\frac{d}{dt}\left(\Delta T_{L23}-\Delta T_{L12}\right)&=4h\frac{\partial\tilde{F}^T}{\partial\tilde{H}}\\ \left(S-\frac{\Delta S_L}{2}\right)\frac{dh}{dt}-\frac{H}{4}\frac{d}{dt}\left(\Delta S_{L23}-\Delta S_{L12}\right)&=4h\frac{\partial\tilde{F}^S}{\partial\tilde{H}}\end{aligned}\right\} \qquad (28)$$

$$\left.\begin{aligned}\Delta T_{L23}-\Delta T_{L12}&=\frac{\partial\Delta T_L}{\partial\tilde{H}}2h\\ \Delta S_{L23}-\Delta S_{L12}&=\frac{\partial\Delta S_L}{\partial\tilde{H}}2h\end{aligned}\right\} \qquad (29)$$

and finally, substitution of the normal modes $(\delta,\varepsilon,h)=(\delta_0,\varepsilon_0,h_0)\exp(\lambda t)$ in equation (28) results in the eiegnevalue equation for H-growth rates:

$$\lambda_H=\frac{4\frac{\partial\tilde{F}^T}{\partial\tilde{H}}}{T-\frac{\Delta T_L}{2}-\frac{H}{2}\frac{\partial\Delta T_L}{\partial\tilde{H}}}=\frac{4\frac{\partial\tilde{F}^S}{\partial\tilde{H}}}{S-\frac{\Delta S_L}{2}-\frac{H}{2}\frac{\partial\Delta S_L}{\partial\tilde{H}}}. \qquad (30)$$

This equation indicates that if fluxes are insensitive to the layer thickness, then λ_H = 0 and the H-merger events cannot occur. This observation may rationalize the absence of H-mergers in the numerical simulations (Figures 9-11).

2. B – Merger

Substitution of the normal modes $(\delta,\varepsilon,h)=(\delta_0,\varepsilon_0,h_0)\exp(\lambda t)$ in (26) results in the eigenvalue equation for growth rates:

$$\left.\lambda_B^2+\frac{4}{H}\left(\frac{\partial\tilde{F}^T}{\partial\tilde{T}}+\frac{\partial\tilde{F}^S}{\partial\tilde{S}}\right)\lambda_B+\frac{16}{H^2}\left(\frac{\partial\tilde{F}^T}{\partial\tilde{T}}\frac{\partial\tilde{F}^S}{\partial\tilde{S}}-\frac{\partial\tilde{F}^S}{\partial\tilde{T}}\frac{\partial\tilde{F}^T}{\partial\tilde{S}}\right)=0\right\} \qquad (31)$$

Since the free coefficient is expected to be small, the positive root can be approximated by

$$\lambda_B = \frac{4}{H}\left\{\frac{\frac{\partial \tilde{F}^S}{\partial \tilde{T}}\frac{\partial \tilde{F}^T}{\partial \tilde{S}} - \frac{\partial \tilde{F}^T}{\partial \tilde{T}}\frac{\partial \tilde{F}^S}{\partial \tilde{S}}}{\frac{\partial \tilde{F}^T}{\partial \tilde{T}} + \frac{\partial \tilde{F}^S}{\partial \tilde{S}}}\right\}. \qquad (32)$$

3. Specific Solutions

Suppose that Turners' 4/3 flux laws are relevant for diffusive convection and can be adopted for the analysis of numerical solutions. (The numerical results generally support this view.) The 4/3 flux law from Turner (1973) has a form

$$\begin{aligned} F_T &= C(R_\rho)\Delta T^{\frac{4}{3}} \\ F_S &= \gamma(R_\rho)F_T \end{aligned} \qquad (33)$$

Substituting (33) into (32) yields

$$\lambda_B = \frac{16(\Delta T)^{1/3}}{H}\left\{\frac{C^2\frac{\partial \gamma}{\partial R_\rho}}{3C'R_\rho - 4C - 3C'\gamma - 3C\gamma'}\right\}. \qquad (34)$$

The last two terms in the denominator of (34) are very small, and therefore can be neglected. This simplifies (34) to

$$\lambda_B = \frac{16(\Delta T)^{1/3}}{H}\left\{\frac{C^2\frac{\partial \gamma}{\partial R_\rho}}{3C'R_\rho - 4C}\right\}. \qquad (35)$$

Since $C'(R_\rho) < 0$, λ_B is positive only if the flux ratio $\gamma(R_\rho)$ decreases with R_ρ. This implies that thermohaline staircases are susceptible to B-merger as long as $\frac{\partial \gamma}{\partial R_\rho} < 0$.

All of our numerical simulations summarized in figure 18 indicate that this condition is satisfied and thereby (35) rationalizes numerous B-merger events as discussed in Chapter II.

On the other hand, since fluxes in (33) are independent of step height, λ_H in (30) is identically zero, which rationalizes the absence of H-merging events in our preliminary numerical simulations.

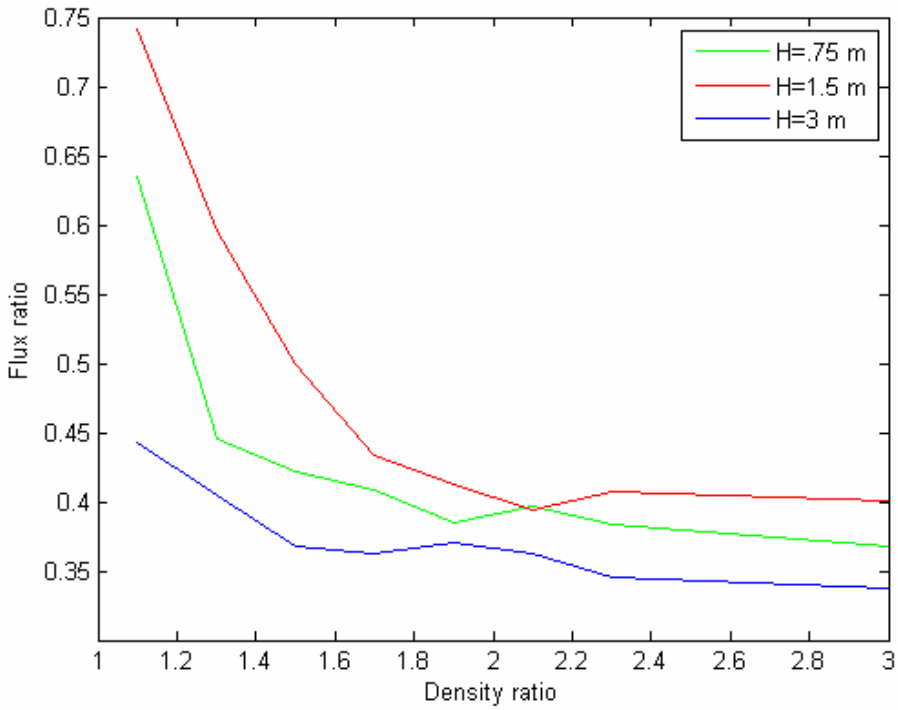

Figure 18. Dependence of λ on R_ρ from one step numerical experiments.

B. PHYSICAL EXPLANATION

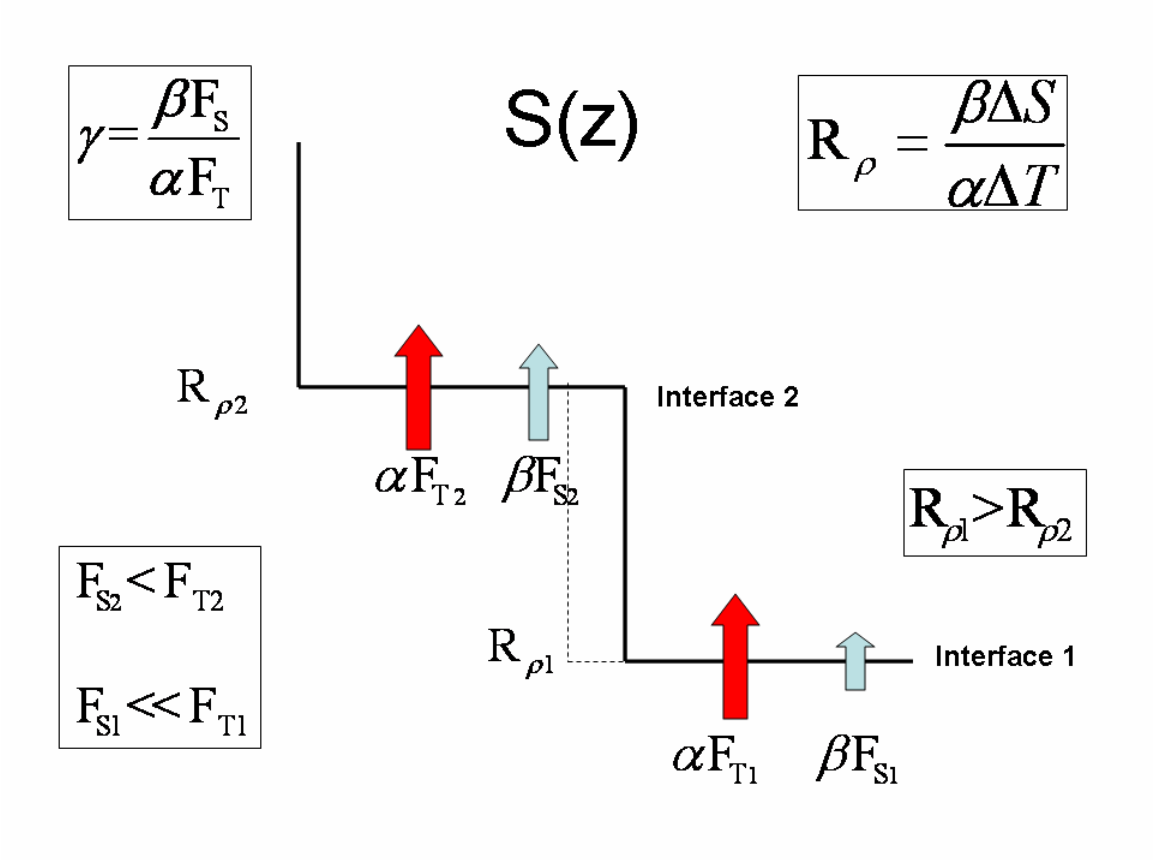

Figure 19. Illustration of B-merger and γ dependence on R_ρ. Depicted is a two-step staircase where F_T and F_s are heat and salinity fluxes, respectively. The dashed line represents erosion of the step due to the greater flux of salt across interface 1 vice 2.

Figure 19 attempts to explain the physical processes involved in B-merger of the thermohaline staircase.

The starting point is a two-step thermohaline staircase. In Figure 18, two steps are almost identical, and the density ratio at interface 1($R_{\rho 1}$) is only slightly greater than the density ratio at interface 2($R_{\rho 2}$).

Diffusive convection is soon established due to the fresh and cold layer overlaying the warm and salty layer, resulting in heat and salinity fluxes, F_T and $F_{s,}$ across the interfaces. Now it is necessary to introduce the idea of dependence of the density on the flux ratio, γ. As Figure 18 illustrates, the flux ratio decreases with the increasing density ratio. Since $R_{\rho 1} > R_{\rho 2}$, it follows that the interface 1 has a slightly lower value of γ than the top interface. Consequently, the salinity flux across the interface 1 is smaller when compared to the interface 2. The net result is the loss of salinity from the bottom step, and subsequent erosion of the bottom step. As salinity flux continues across the interfaces, it decreases across the interface 1 and increases across the interface 2, thus causing an increase of ΔS across the interface 1 and decrease of ΔS across the interface 2. This in turn causes R_ρ across the interface 1 to become even greater, and R_ρ across the interface 2 becomes even smaller. As salinity flux continues to increase across the interface 2, so does the value of γ for the same interface. Similarly, the salinity flux for the interface 1 continues to decrease, and so does the value of γ for that interface.

This positive feedback leads to the complete erosion of the weaker interface 2. The proposed mechanism is consistent with both merging theorem (35) and with the earlier (Chapter II) numerical simulations.

THIS PAGE INTENTIONALLY LEFT BLANK

IV. THEORY-BASED ANALYSIS OF THE DIRECT NUMERICAL SIMULATIONS

A. TURNER'S FLUX LAW MODEL

1. Verification of the 4/3 Flux Law

The 4/3 flux law, first introduced in Chapter I, is used in calculating of the oceanic diffusive fluxes since their direct measurements are rarely available. Therefore, estimates are made from measuring ΔT and calculating C empirically, then substituting into (4). If the 4/3 flux law applies to our numerical calculations, then the quantity $\frac{F_{T\,\dim}}{(T_{\dim})^{\frac{4}{3}}}$ showed in Table 3 should depend largely on R_{ρ} but not on H.

To test the 4/3 flux law, the results from the series of one step numerical experiments introduced earlier were analyzed. The fully equilibrated results of numerical simulations were used, and the averaged heat flux was computed based only on the second half of the experiment. The goal was to exclude the large initial fluctuations of diffusive fluxes and use only the equilibrated results. The typical non-dimensional fluxes from a one-step numerical experiment are displayed in Figure 20. Note the initial spike in the flux values.

The magnitudes of non-dimensional fluxes obtained from each experiment were first dimensionalized using (7) and (8). Since there is a linear relationship between ΔT and

ΔH, both quantities are equivalent ($\frac{\partial \overline{T}}{\partial z}$ is constant in our model) and ΔH (vertical step scale) was used in equation (4). The results are summarized in Table 3.

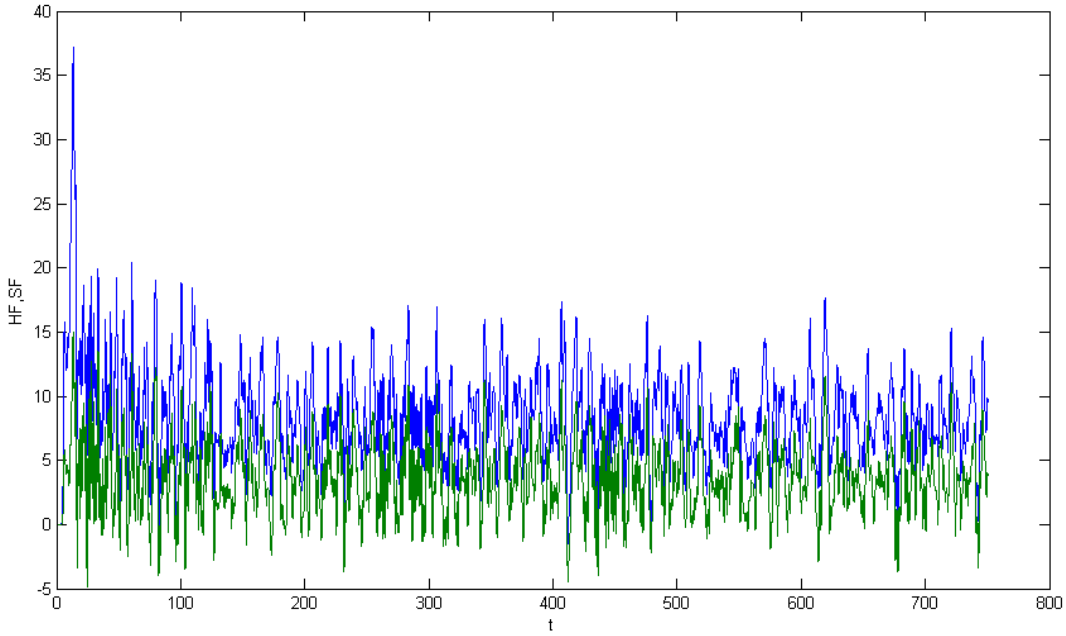

Figure 20. Time plot of non-dimensionalized diffusive fluxes from a numerical experiment. The blue curve and green curve represent heat and salinity flux, respectively.

H (m)	R_ρ									
	1.1	1.3	1.5	1.7	1.9	2.1	2.3	3.0	4.0	5.0
0.75	.774	.357	.258	.161	.113	.085	.061	.038	.024	.015
1.5	.758	.285	.211	.162	.122	.101	.103	.057	0.45	.037
3.0	.544	-	.157	-	-	-	.083	.035	-	.023

Table 3. $\frac{F_{T\,\dim}}{(T_{\dim})^{\frac{4}{3}}}$ as a function of the density ratio, R_ρ and the layer thickness (m). Dashes indicate no values were obtained due to the computational constrains.

An analysis of the results from Table 3 reveals that the 4/3 flux law works reasonably well for our numerical experiments as the values of heat flux depend more on R_ρ and less on H.

2. Comparison of Numerical Fluxes with Fluxes Computed from Oceanic Data

There is some disagreement between the magnitude of diffusive fluxes that are computed using the laboratory derived flux laws and the fluxes computed using actual oceanic observation. If the diffusive heat fluxes for the Arctic are on the order of magnitude 2 to 6 W m^{-2}, as calculated by Wilson (2007), they could play a significant role in the Arctic heat budget and contribute to the melting of the Arctic ice cap.

Padman and Dillon (1987) reported that based on the data collected from the Beaufort Sea during the Arctic Internal Wave Experiment (AIWEX) in March-April 1985, the

heat fluxes estimated from laboratory-derived flux laws ranged from 0.02 to 0.1 W m^{-2} which is one to two order of magnitude smaller than the alternative heat flux estimates. Padman (1994) estimates vertical heat fluxes through thermohaline steps to be between 2 and 5 W m^{-2} using flux laws proposed by Kelley (1990) and Marmorino and Caldwell(1976). His findings are derived from the data collected near the Yermak Plateau as a part of the Coordinated Eastern Arctic Experiment(CEAREX) in 1989. Based on the analysis of the Ice-Tethered Profiler data obtained from Woods Hole Oceanographic Institute and the Beaufort Gyre Exploration Program, heat fluxes calculated using Turner's 4/3 flux laws range from 2 to 6 W m^{-2} (Wilson, 2007).

However, as Padman and Dillon (1988) point out, laboratory experiments differ in a number of ways from the actual ocean. For example, much greater fluxes are required to minimize wall heat losses, and there is a possibility of secondary circulations driven by the tank geometry on the laboratory side; additionally there is the potential for significant interaction between double diffusion and instabilities driven by ambient shear. Also, laboratory derived flux laws (Turner, 1973) may not be the ideal tool to use in estimating diffusive fluxes found in oceanic staircases. Therefore, it is reasonable to question the assumption that the values of diffusive heat fluxes obtained from laboratory experiments can be extrapolated to the actual oceanic conditions.

Another interesting angle to consider is the value of the molecular diffusivity ratio. As mentioned in Chapter II,

the numerical experiments relevant to this thesis used the molecular diffusivity ratio $\tau = 1/10$. As it was explained earlier, this was done for numerical convenience and should not significantly affect the physics and dynamics of the diffusive convection. It is, however, highly desirable to take into account dependence of fluxes on τ, which was done as follows.

Takao and Narusawa (1980) conducted a study with substances of different molecular diffusivity ratio, τ, and concluded that the substance with the lowest value of τ registered the highest flux ratio. They suggested that the heat fluxes across the diffusive interface should scale as $\tau^{-0.71}$. Thus the value of the diffusive fluxes would have to increase by a factor of 5.13 (scaling the value of $\tau = 0.1^{-0.71}$ in the numerical experiments). In addition, in order to obtain equivalent values, each numerical experiment was extrapolated, using the 4/3 flux law, to the step height of 5 m, the average step height of the Beaufort Gyre Arctic staircase (Wilson, 2007) Table 4 summarizes the results after applying this correction.

H (m)	R_ρ									
	1.1	1.3	1.5	1.7	1.9	2.1	2.3	3.0	4.0	5.0
0.75	33.8	15.6	2.20	11.3	5.1	3.7	2.7	2.7	1.0	0.9
1.5	33.3	12.3	1.80	9.23	5.3	4.7	4.5	2.5	1.6	1.6
3.0	18.1	-	5.28	-	-	-	3.4	1.9	-	0.9

Table 4. Heat flux (W m^{-2}), corrected by the factor of 5.13, as the function of the density ratio, R_ρ, and the layer thickness, H (m). Dashes indicate no values were obtained due to the computational constraints.

Comparison of the results from Table 4 to the diffusive fluxes determined from oceanic observations by Wilson (2007), reveals that both numerical and oceanic heat fluxes are in the same order of magnitude. This raises the question of using the higher value of τ in the numerical simulations of diffusive heat fluxes. It is reasonable to assume that the higher value of τ adversely affects the numerically determined diffusive heat fluxes and warrants future exploration.

B. APPLICATION OF THE MERGING THEOREM

Next, we proceed to determine how well the merging theorem predicts the timing of merging events was performed. The same series of numerical experiments which was used to verify merging of layers was used in this analysis. As expected, the value of heat flux decreased as the value of R_ρ increased as presented in Table 1. Next, the magnitudes of non-dimensional heat fluxes F_T were plotted as a function

of R_ρ, and the curve fitting was performed using Matlab curve fitting tool in order to determine the formula describing the coefficient C in formula (35). Based on the best fit, a formula was obtained

$$C = 6.2\exp(-3.17R_\rho) \qquad (36)$$

Substituting (36) into (35) yields

$$\lambda_B = \left\{\frac{153\exp(-6.24R_\rho)}{9.5R_\rho + 4}\right\}. \qquad (37)$$

This form of λ_B predicts the time scale for a particular merging event for the numerical experiments with an initial step size of 0.75. The inverse of λ_B gives time in non-dimensional units. The time scale was computed using formula (37) and compared to the time scale determined from numerical experiments. The results are summarized in Table 5.

R_ρ	λ_B theory	λ_B actual	t theory (non-dim.)	t actual (non-dim.)	t actual (days)
1.1	0.0111	0.01	90.1	100	.80
1.2	0.0056	0.008	178.5	125	1.0
1.3	0.0028	0.0029	357.1	340	2.7
1.4	0.0014	0.0011	714.3	910	7.1

Table 5. Comparison of merging theorem with numerical experiment.

In analyzing the values in Table 5, it is evident that the merging theorem predicts the time scale of merging events reasonably well, always within the order of magnitude. The verification of merging theorem for higher values of R_ρ was not performed due to the computational constraints; each increase of R_ρ by one tenth of a point results in an approximate doubling of the time scale. Future studies should expand the verification of merging theorem for the higher values of R_ρ.

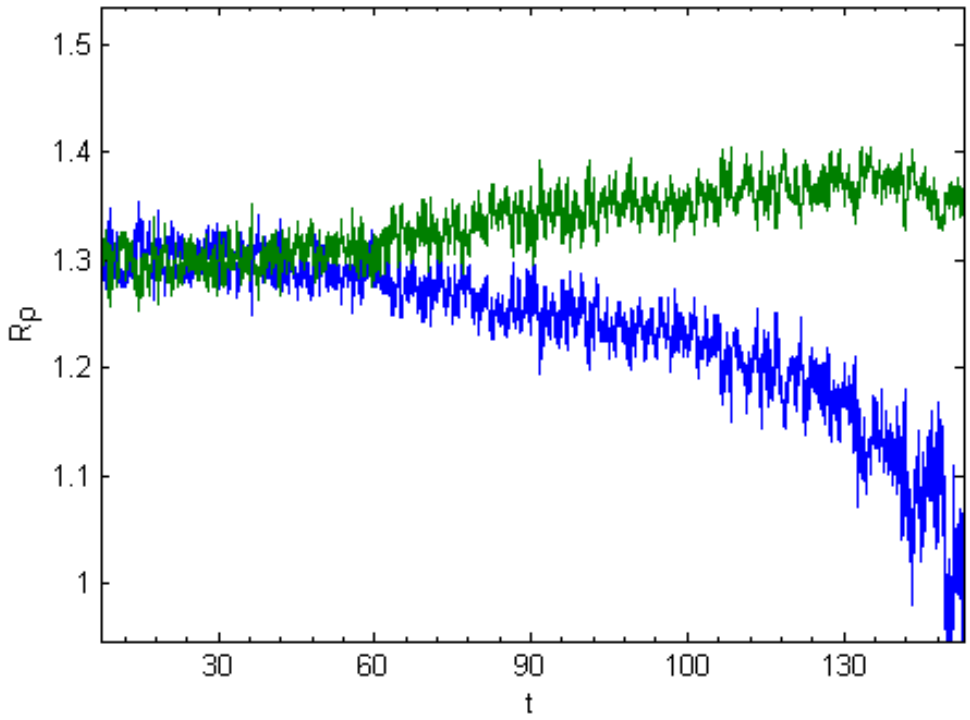

Figure 21. Variation of R_ρ across two different interfaces in a two-step numerical experiment. The green (blue) curve represents the higher (lower) initial value of R_ρ.

The physical principles described in Chapter IV confirmed the results in Figure 21, where we plot the same

records of the density ratios at two interfaces in a two-step experiment with the overall R_ρ=1.3 and H=3 m. Note the continuous increase (decrease) of the green (blue) curve representing the higher (lower) value of the density ratio at t=60 after the initial fluctuations. Also note a sharper decrease in the lower value of R_ρ at t=100 represented by the blue curve until the curve reaches R_ρ=1, the moment when merging occurs.

THIS PAGE INTENTIONALLY LEFT BLANK

V. RESULTS AND CONCLUSIONS

The double-diffusive process has received a considerable amount of attention due to its effect on various large oceanic features. This study is mainly focused on the dynamics of diffusive convection, particularly the numerical modeling of the dynamics of thermohaline staircases and associated diffusive fluxes. This study uses the results of the study of oceanic data from the Beaufort Gyre (Wilson, 2007) in order to compare the magnitude of the diffusive heat flux and to analyze its significance on the Arctic thermal budget.

In order to compare the numerically computed diffusive heat fluxes to the fluxes computed from oceanic data, the 4/3 flux is invoked (Turner, 1973). The validity of the 4/3 flux was tested first for the numerical solution. The results are summarized in Table 3. The analysis revealed that the 4/3 flux law works reasonably well for the steps < 3 m, but the amplitude needs adjustment.

Padman (1994) and Muench et al (1990) concluded that diffusive convection could play a significant role in influencing the vertical heat fluxes from the warm and salty intermediate water upwards to the polar mixed layers and sea ice. However, the results from the laboratory experiments put the value of the vertical diffusive heat flux on the order of 10^{-2} to 10^{-1}, a non-significant value in the total Arctic heat budget. Nevertheless, it is necessary to consider that the laboratory experiments differ in many ways from the actual oceanic conditions. Diffusive heat fluxes computed from oceanic data from the Beaufort Gyre range from

2 to 6 W m^{-2} (Wilson, 2007), a value which is large enough to play a significant role in the Arctic heat budget.

The computed values of the diffusive heat fluxes range from 1 to 3 W m^{-2} for $3<R_\rho<5$ and are summarized in Table 4 These values are comparable to the heat fluxes computed from the actual oceanic data. However, the values of numerically computed heat fluxes are up to an order of magnitude greater than the results from the laboratory solutions. Since there is large discrepancy among these results, more study is necessary before the final assessment of the role of the diffusive vertical fluxes in the maintenance of the Arctic thermocline can be made.

In addition to computations of diffusive fluxes, this study offers some insight into the dynamics of thermohaline staircases. The merging theorem (Radko 2007) predicts types and scales of merging realized in the thermohaline staircases. The results of this study confirm that interfaces within the diffusive staircase erode over time without any vertical motion, confirming the merging theorem prediction that only B-type merger is taking place.

The quantitative predictions of the merging theorem were tested as well and are summarized in Table 5. Based on these results, the numerical experiments confirm that the merging theorem predicts the time scale of merging events within an order of magnitude. Due to the computational constraints, only verification for the lower values of R_ρ was performed. Since diffusive convection is favorable for

the regions with $2<R_{\rho}<10$ and 2<H<7 m, future studies should focus on a more complete exploration of this parameter range.

THIS PAGE INTENTIONALLY LEFT BLANK

LIST OF REFERENCES

Aagaard K., Greisman, P. (1975). Toward new mass and heat budgets for the Arctic Ocean. *J. of Gepphysical Res.*, 80, 3821-3827.

Balmforth, N. J., Llewellyn Smith, S. G., Young, W. R. (1998). Dynamics of interfaces and layers in a stratified turbulent fluid. *J. Fluid Mech.*, 355, 329-358.

Kelley D. E. (1984). Effective diffusivities within oceanic thermohaline staircases. *J. of Gepphysical Res.*, 89, 10484-10488.

Kelley, D. E. (1990). Fluxes through Diffusive Staircases: A new formulation. *J. of Geophysical Res.*, 95, 3365-3371.

Marmorino G. O.and Caldwell, D. R. (1976). Heat and salt transport through a diffusive thermohaline interface. *Deep-Sea Res.*, 23, 59-67.

Merryfield W. J.(2000). Origin of thermohaline staircases. *J. of Physical Oceanography,* 30, 1046-1068.

Muench, R. D., Fernando, H. J. S., Stegun, G. R.(1990). Temperature and salinity staircases in the northwestern Weddel Sea. *J. Phys. Oceanography,* 20, 295-306.

Padman, L., Dillon, T. M. (1987). Vertical heat fluxes through the Beaufort Sea thermohaline staircase. *J. of Geophysical Res.*, 92, 10799-10806.

Padman, L. (1994). Momentum fluxes through sheared oceanic thermohaline steps. *J. of Geophysical Res.*, 99, 22491-22499.

Padman, L., Dillon, T. M. (1988). On the Horizontal Extent of the Canada Basin Thermohaline Steps. *J. of Physical Oceanography,* 18, 1458-1462.

Radko, T., and Stern, M. E. (1999). Salt fingers in three dimensions. *J. Mar. Res.* 57. 471-502.

Radko, T. (2003). A mechanism for layer formation in a double-diffusive fluid. *J. Fluid Mech.*, 497, 365-380.

Radko, T. (2005). What determines the thickness of layers in a thermohaline staircase? *J. Fluid Mech.*, 523, 79-98.

Radko, T. (2007). Mechanics of merging events for a series of layers in a stratified turbulent fluid. *J. Fluid Mech.*,577, 251-273.

Ruddick, B. R. (1983). A practical indicator of the stability of the water column to double-diffusive activity. *Deep-Sea Res.,* 30, 1105-1107.

Schmitt, R. W. (1990). On the density ratio balance in the Central Water. *J. of Physical Oceanography,* 20, 900-906.

Schmitt, R. W. (1994). Double diffusion in oceanography. *Annu. Rev. Fluid Mech.,* 26, 255-285.

Schmitt, R. W., Ledwell, J., Montgomery, E.T., Polzin, K., Toole, J.(2005). Enhanced diapycnal mixing by salt fingers in the main thermocline of the tropical Atlantic. *Science,* 306, 385-388.

Stern, M. E. (1960). The “salt fountain” and thermohaline convection. *Tellus,* 12, 172-175.

Stern, M. E. (1969). Collective instability of salt fingers. *J. Fluid Mech*., 35, 209-218.

Stern, M. E., and Radko, T. (1998). The salt finger amplitude in unbounded T-S gradient layers. J. Mar. Res., 56, 157-196.

Stern, M. E., Radko, T., Simeonov, J. (2001). 3D salt fingers in an unbounded thermocline with application to the Central Ocean. *J. Mar. Res.*, 59, 355-390.

Stommel, H .M., Arons,A. B., Blanchard, D. (1956). An oceanographic curiosity: The perpetual salt fountain. *Deep-Sea Res.,* 3, 152-153.

Takao, S., and Narusawa, U. (1980). An experimental study of heat and mass transfer across a diffusive interface. *Int. J. Heat Mass Transfer,* 23, 1283-1285.

Turner, J. S. (1965). The coupled turbulent transports of salt and heat across a sharp density interface. *Int. J. Heat Mass Transfer,* 6, 759-767.

Turner, J. S. (1973). *Buoyancy Effects in Fluids.* Cambriddge University Press, Cammbridge, UK, 276pp.

Wilson, A. L. (2007). Structure and Dynamics of the thermohaline staircases in the Beaufort Gyre. Unpublished Master of Science in Meteorology and Physical Oceanography Thesis, Naval Postgraduate School, Monterey, CA.

You, Y. (2002). A global ocean climatological atlas of the Turner angle: Implications for double-diffusion and water-mass structure. *Deep-Sea Res.,* 49, 2075-2093.

THIS PAGE INTENTIONALLY LEFT BLANK

INITIAL DISTRIBUTION LIST

1. Defense Technical Information Center
   Ft. Belvoir, Virginia

2. Dudley Knox Library
   Naval Postgraduate School
   Monterey, California

3. Dr. Mary L. Batteen
   Naval Postgraduate School
   Monterey, California

4. Dr. Timour Radko
   Naval Postgraduate School
   Monterey, California

5. Dr. William Shaw
   Naval Postgraduate School
   Monterey, California